Quantum kinetic theory. VI. The growth of a Bose-Einstein condensate

M. D. Lee and C. W. Gardiner
School of Chemical and Physical Sciences, Victoria University, Wellington, New Zealand
(Received 20 December 1999; published 11 August 2000)

A detailed analysis of the growth of a Bose-Einstein condensate is given, based on quantum kinetic theory, in which we take account of the evolution of the occupations of lower trap levels, and of the full Bose-Einstein formula for the occupations of higher trap levels, as well as the Bose-stimulated direct transfer of atoms to the condensate level introduced by Gardiner *et al.* [Phys. Rev. Lett. **79**, 1793 (1997); **81**, 5266 (1998)]. We find good agreement with experiment at higher temperatures, but at lower temperatures the experimentally observed growth rate is somewhat more rapid. We also confirm the picture of the ''kinetic'' region of evolution, introduced by Kagan, Svistunov, and Shlyapnikov (Zh. Eksp. Teor. Fiz. **101**, 528 (1992) [Sov. Phys. JETP **75**, 387 (1992)]), for the time up to the initiation of the condensate. The behavior after initiation essentially follows our original growth equation, but with a substantially increased rate coefficient. Our modeling of growth implicitly gives a model of the spatial shape of the density profile of the condensate-vapor system as the condensate grows, and thus provides an alternative to the present phenomenological fitting procedure, based on the sum of a zero-chemical potential vapor and a Thomas-Fermi-shaped condensate. Our method gives substantially different results for condensate numbers and temperatures obtained from phenomenological fits, but fits the published column density data very well.

PACS number(s): 03.75.Fi, 05.30.Jp, 51.10.+y

I. INTRODUCTION

Although the race to produce a Bose-Einstein condensate was preceded by intense debate concerning the likely rate of its formation, the discovery that a Bose-Einstein condensate of alkali-metal atoms could be produced relatively simply [1–3], and that the growth time was of the order of one second, moved most theoretical activity into the investigation of the properties of the condensates so produced. Since the production of the first Bose-Einstein condensate there have been few theoretical investigations into condensate growth, and only one experiment [4] has made any measurements of growth rates. Only the work of the present authors and co-workers, based on quantum kinetic theory, has made quantitative predictions on the growth rate of a Bose-Einstein condensate. This work started when we showed how to introduce the concept of stimulated condensate growth resulting from kinetic processes [5], leading to a very simple formula for the growth rate. The MIT experiment [4] took the form of a verification of the validity of our theoretical prediction. At the same time, in Ref. [6] we refined the basic concept of bosonic stimulation to generate a less idealized theoretical picture, and to compare it with experiment. These initial papers were of necessity brief, and developed neither the full theoretical justification on the numerical modeling nor the full range of possible comparison with the available experimental data. In particular, no account was taken of the information available on the spatial distribution of the atoms in the vapor-condensate system as the condensate grows from the vapor.

This paper will therefore give the detailed justifications and a full range of comparison with experimental data. Most particularly, we want to present a theoretically justifiable method of describing the condensate vapor system as it grows. The absence of such a description has led to a phenomenological fitting of vapor profiles to a *zero chemical potential* Bose-Einstein distribution in the MIT growth experiment [4,7] (and as well in the experiments on Bose-Einstein condensate in hydrogen [8]), which may be an imperfect model whose results could well be misleading.

The theoretical description of condensate growth that we present is largely able to be viewed as a modification of the quantum Boltzmann equation, in which, however, explicit note is taken of the modification of the excitation spectrum by the existence of the condensate, including of course the fact that the lowest single-particle excitation energy is the chemical potential $\mu_C(n_0)$ of the condensate of n_0 atoms. Equilibrium arises as a result of the equality of the chemical potentials of uncondensed vapor and condensate, a picture which is rather similar to that normally adopted for chemical reactions. The quantum Boltzmann equation itself automatically provides the Bose stimulation, which makes transition rates into the condensate and other highly occupied levels achieve a speed which permits the production of the condensate in a finite time. Without Bose stimulation, the production of a condensate of about 1 000 000 sodium atoms would take 30 h, rather than the 100 ms observed.

At first glance it might appear that a description which appears to be based on the quantum Boltzmann equation would have nothing to say about condensate coherence or the origin of that coherence. This is emphatically not the case—the kinetics of the transfer of the atoms between energy levels *in a trap* requires the existence of a wave function for each energy level. The condensate level has its own wave function, and this obeys the Gross-Pitaevskii equation. The coherence arises because this level becomes macroscopically occupied. There is no *precise* moment when one can say that the condensate initiates. This picture applies in a trap, in which the energy levels about which we have been speaking are rather well separated. The picture of a Bose-Einstein condensate, as developed in the middle part of this century as a part of condensed-matter theory, is of a homogeneous and thus infinitely extended system—a system for which the thermodynamic limit is achieved. Looked at from our view-

point, this would be achieved by making the trap broader and ultimately flat. There is a transition point where the trap becomes so flat that there is an occupation of the lowest quasiparticle levels which becomes comparable to the occupation of the condensate itself. At this stage the traditional condensed matter picture becomes relevant, but this is not achieved in any traps presently in use.

II. MODEL FOR GROWTH OF A CONDENSATE

In this section, the formalism of quantum kinetic theory [9] will be used to form a model of the growth of a trapped Bose-Einstein condensate. The Bose atoms are described by a second-quantized field, in the pseudopotential approximation; that is, we write

$$H = H_{\rm kin} + H_I + H_T, \tag{1}$$

where

$$H_{\rm kin} = \int d^3\mathbf{x}\, \psi^\dagger(\mathbf{x}) \left(-\frac{\hbar^2}{2m}\nabla^2 \right) \psi(\mathbf{x}), \tag{2}$$

$$H_I = \frac{u}{2} \int d^3\mathbf{x}\, \psi^\dagger(\mathbf{x}) \psi^\dagger(\mathbf{x}) \psi(\mathbf{x}) \psi(\mathbf{x}), \tag{3}$$

and the term H_T arises from a trapping potential as

$$H_T = \int d^3\mathbf{x}\, V_T(\mathbf{x}) \psi^\dagger(\mathbf{x}) \psi(\mathbf{x}). \tag{4}$$

The pseudopotential method is used—its validity for this kind of system was justified in QKV—where $u = 4\pi a \hbar^2/m$, and a is the s-wave scattering length arising from the interatomic potential.

The situation being considered is that of a vapor cloud confined in a trap in which the lower-energy levels are not significantly populated, while the higher-energy levels contain thermalized equilibrium populations, characterized by a temperature T and chemical potential μ, unstable against condensate formation.

This situation is likely to arise, to a degree of approximation, if a system, which is initially in equilibrium at a temperature slightly greater than the critical temperature, is cooled very suddenly to a temperature below the critical temperature, by removing the very high-energy atoms in a rapid evaporative cooling ''cut.'' The higher-energy levels will very quickly come to their equilibrium distributions, since the difference between the distributions before and after the cut are quite small at the higher energies. However, the lower levels will be far from equilibrium and evolve to form a condensate. This is possibly one of the easiest scenarios to model, it is also the situation investigated by the only detailed experimental study of the growth of a condensate in a gas of ^{23}Na atoms [4].

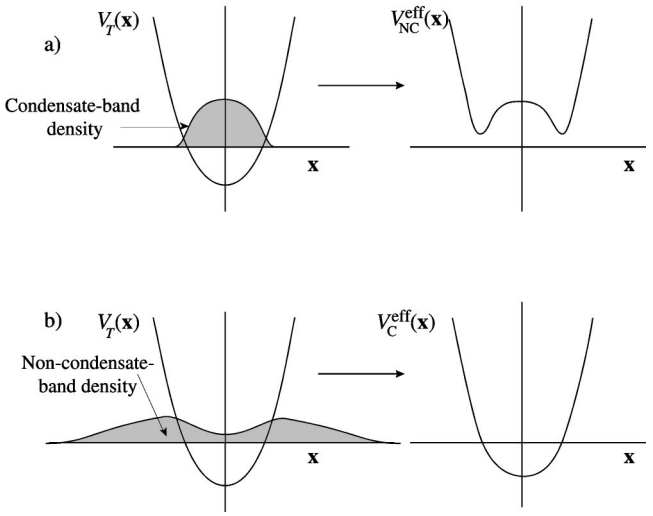

FIG. 1. Representation of the modification of the trapping potential for (a) the noncondensate band and (b) the condensate band due to mean-field effects.

A. System

The system is contained in a three-dimensional harmonic potential, characterized by the frequencies ω_x, ω_y, and ω_z. It will be useful to define the geometrical mean frequency of the trap as $\omega = (\omega_x \omega_y \omega_z)^{1/3}$.

1. Effective potentials arising from mean-field effects

In this system the energies and wave functions of the lower trap levels are quite strongly affected by the presence of the condensate, and the effect will of course change as the condensate grows. In QKV it was shown that it is reasonable to account for this by introducing mean-field effects, which make the effective potentials depend on the occupations of the bands. The situation is illustrated in Fig. 1. As the condensate grows, it expels the vapor from the center of the trap, and this expulsion serves to reduce the mean field of the vapor as experienced by the condensate. The growth will be assumed to be so slow that the condensate and noncondensate bands are always in *thermal* equilibrium—that is, they will have a well-defined temperature shared by both of them, but will not have the same chemical potential. Growth therefore occurs as atoms are transferred from the vapor to the condensate, leading eventually to a unique chemical potential for the whole system.

2. Condensate and noncondensate bands

In the formalism of quantum kinetic theory, the system is divided into condensate and noncondensate bands. In this paper we will treat the situation in which the noncondensate band is assumed to be in thermal equilibrium with a temperature T and chemical potential μ, and to contain the vast majority of the atoms so that it is essentially undepleted by the process of condensate formation.

The picture of growth we will use is that presented in QKV. In that paper, it was shown that a legitimate division

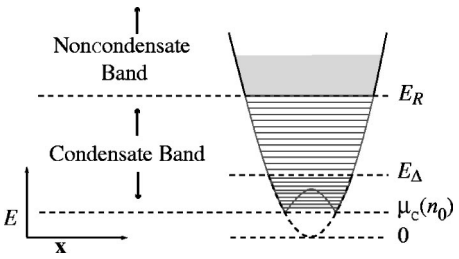

FIG. 2. Schematic representation of the simple model to change the energy levels due to the mean field effects of the condensate. Levels are evenly distributed between E_Δ and $\mu_C(n_0)$ which increases with n_0. The levels appropriate to the effective potential are approximated by a uniform distribution between the lowest-energy level and the value E_Δ.

into condensate and noncondensate bands can be made in which one distinguishes between *particlelike* excitations, to which it is possible to assign a definite number of atoms, and *phononlike* excitations, which are collective modes, which normally involve a large average number of atoms, but are not eigenstates of the atom number. In practice, it has been shown [15] that the energy above which all excitations are essentially particlelike is relatively small. For the purposes of our modeling, however, there are two criteria which must be considered in the definition of the condensate band.

(i) The noncondensate band is considered to be time independent; therefore, the condensate band must include all levels whose populations change significantly during the condensate growth process. For the noncondensate band, the thermal distribution is given in the bulk by $[e^{(E-\mu)/kT}-1]^{-1}$. This is only valid for $E>\mu$, and gives very large populations when $E\approx\mu$. The transition rates in and out of levels in this vicinity also become very large, which contradicts the assumption that the distribution of the noncondensate band is time independent. These lower states therefore *must* be treated time dependently, and hence must be included in the condensate band.

(ii) The condensate band consists principally of levels whose energy eigenvalues are significantly affected by the presence of a condensate—but levels which are not affected may be included if this is desirable, which must be done if the first criterion is to be met.

Consequently, in this paper we will choose the condensate band to consist of all levels with energy less than the value E_R. We will also introduce an energy $E_\Delta<E_R$, which is the energy above which we can consider the energy levels to be unaffected by the condensate, as illustrated in Fig. 2.

3. Grouping of energy levels into bands

The inclusion of all the condensate band energy levels in the model means that simulations of the system require, in principle, the calculation of all the eigenfunctions of the condensate band, and detailed summations over these. In practice the number of energy levels involved is of the order of tens of thousands, which makes an exact description impractical. However, progress can be made by grouping together energy levels in the condensate band into small ''subbands,'' with only the ground state (condensate state) being described as a single level. Each subband is described by an energy e_m and contains all the eigenstates found within the energy range $[e_m-\Delta e_m/2, e_m+\Delta e_m/2]$. The value of Δe_m is chosen partially by the requirement that the lowest of these subbands contains at least three levels. Smaller values of Δe_m would lead subbands containing only fractions of individual levels, which is obviously unphysical. As the condensate grows, the mean-field effects from the high occupation of the condensate level will cause the energies of the levels in the subbands to increase. The values of e_m and Δe_m are therefore dependent on the condensate occupation, and the manner in which they are altered will be discussed later.

B. Notation

For clarity, we set out some of our notation:

N: number of atoms in the *condensate band*, (5)

n_0: number of atoms in the *condensate*, (6)

$n_{0,f}$: *equilibrium* number of atoms in the *condensate*, (7)

$\mu_C(n_0)$: chemical potential of the *condensate*, (8)

μ: chemical potential of the *noncondensate band*, (9)

$\xi_{n_0}(\mathbf{x})$: wave function of an n_0 atom condensate. (10)

In the situations we will consider, the number of condensate atoms n_0 will vary from zero to almost N, but this will always be substantially less than the number of atoms in the whole system, composed of both condensate and noncondensate bands. Thus when the condensate is fully grown, the approximation $n_0\approx N$ will be valid, and will often be used.

C. Density of states for the system

In the absence of any condensate, the density of states $G(E)$ is taken to be that of a non-interacting gas in a harmonic well. That is

$$G(E)\equiv\frac{dN(E)}{dE}=\frac{\left(E-\frac{3}{2}\hbar\bar{\omega}\right)^2}{2\hbar^3\omega_x\omega_y\omega_z}, \tag{11}$$

where $N(E)$ is the cumulative number of states with energy less than E and $\bar{\omega}=(\omega_x+\omega_y+\omega_z)/3$. The number of states in the subband with average energy e_m is thus $g_m=G(e_m)\Delta e_m$. The energy scale is such that the value of $V_T(\mathbf{r})=m(\omega_x^2x^2+\omega_y^2y^2+\omega_z^2z^2)/2$ is zero at the origin.

Once the condensate begins to form, the mean-field effects need to be taken into account. The mean-field repulsion due to the condensate changes the energies of the lower trapped states. The energy of the condensate level is equal to

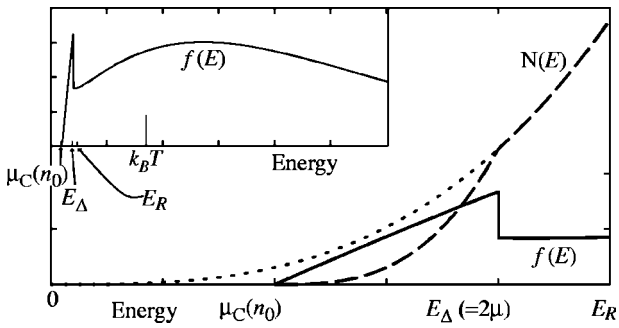

FIG. 3. The cumulative number of states for a gas in a harmonic potential well. The dotted line shows the situation for a noninteracting gas (no mean field effects). The dashed line represents the cumulative number of states due to the simple model proposed in the text to incorporate mean field effects. The solid line shows the corresponding occupation per energy interval $f(E) = G(E)[\exp((E-\mu)/kT)-1]^{-1}$, also shown on a larger scale in the inset.

the chemical potential $\mu_C(n_0)$, which increases with n_0. In the Thomas-Fermi approximation the rise is proportional to $n_0^{2/5}$. Obviously the condensate level must remain the lowest-energy state, and thus the energies of the other states below E_Δ must also rise in some fashion. The exact nature of the energy change is difficult to calculate, but some reasonable approximations can be proposed which should reproduce the significant behavior caused by the mean-field effects.

The most simply calculated estimate of the energy changes is to assume the energies of the subbands e_m are evenly distributed between the fixed upper limit of E_Δ and the lower limit of $\mu_C(n_0) \approx \alpha n_0^{2/5}$. This is illustrated schematically in Fig. 2. Both the values of e_m and the values of Δe_m are now n_0 dependent.

The final value of Δe_m (after the growth of the condensate) is set to be $\hbar\omega$. This condition also always fulfills the requirements that there are at least about three discrete levels contained in the lowest-energy subband, and yet ensures that the subband has only a relatively small energy range.

The density of states for the condensate band, in the presence of the condensate, is thus taken to be approximately $G_{n_0}(E) = \mathcal{N}[E-\mu_C(n_0)]^2$, where $\mathcal{N}$ is a normalization chosen so that the cumulative number of states at E_Δ is the same as for the noninteracting harmonic-oscillator potential. This behavior is illustrated in Fig. 3. As the discontinuity at E_R shows, this model is obviously quite simplistic, and more realistic models will be discussed later.

It should be noted that in the inset of Fig. 3 the number of particles per energy interval $f(E)$ is shown (the occupation of the condensate level is not shown) for equilibrium conditions. From this inset it can be seen that the vast majority of atoms do indeed reside at energies higher than E_R, and so the assumption that the noncondensate band is undepleted should be valid.

1. Modified Thomas-Fermi chemical potential

In the Thomas-Fermi approximation, the chemical potential of the condensate is given by

$$\mu_C(n_0) = \left(\frac{15a\omega_x\omega_y\omega_z m^{1/2}\hbar^2}{2^{5/2}} n_0 \right)^{2/5}, \tag{12}$$

which vanishes as $n_0 \to 0$. However, the ground state of a noninteracting gas in a harmonic well is $\hbar(\omega_x+\omega_y+\omega_z)/2$, and so the real chemical potential should approach this value as $n_0 \to 0$. In order to interpolate the Thomas-Fermi chemical potential to satisfy this requirement, the following form for the chemical potential will be used:

$$\mu_C(n_0) = \alpha(n_0+\nu)^{2/5}, \tag{13}$$

where $\alpha = (15a\omega_x\omega_y\omega_z m^{1/2}\hbar^2/4\sqrt{2})^{2/5}$, and ν is a constant such that $\alpha\nu^{2/5} = \hbar(\omega_x+\omega_y+\omega_z)/2$.

2. Estimate of E_Δ

An estimate for the value of E_Δ, above which the excitation spectrum is well described by that for a noninteracting gas, can be obtained using the number-conserving Bogoliubov spectrum [16,12]. The quantity of interest now is the ratio of the corrections to the energy level arising from the presence of the condensate, to the energy level determined by the noninteracting gas model. For the case of the trap used in the ^{23}Na growth experiments at MIT [4], numerical calculations show that the ratio is less than 10% for energies $\geqslant 2\mu_C(n_0)$, and the corrections are of the order of only 5% for $E \sim 2.5\mu_C(n_0)$. Thus a reasonable estimate of E_Δ to be used in the simulations is

$$E_\Delta = 2\mu_C(n_{0,f}), \tag{14}$$

where $n_{0,f}$ is the equilibrium occupation of the condensate level, and this is the value of E_Δ that will be used in this paper.

3. Comparison with more accurate density of states

As a result of the predominantly single particle nature of the excitation spectrum, the cumulative number of states $\mathrm{N}(E)$ is expected to be quite well described at high energies by the semiclassical approximation

$$\mathrm{N}(E) = \frac{1}{(2\pi\hbar)^3}\int_0^E d\varepsilon \int d\mathbf{r}\int d\mathbf{p}\ \ \delta(\varepsilon - E_{\mathrm{sp}}(\mathbf{p},\mathbf{r})), \tag{15}$$

where $E_{\mathrm{sp}}(\mathbf{p},\mathbf{r}) = p^2/2m + V_T(\mathbf{r}) + (8\pi\hbar^2 a/m)|\xi_{n_0}^2(\mathbf{r})| - \mu_C(n_0)$ is the semiclassical energy of a single particle in the potential created by the combination of the trapping potential and the mean-field repulsion of the condensate. Equation (15) thus represents the summation over all phase-space cells which contain a single-particle excitation state of energy less than E. In Ref. [16], by carrying out the momentum and space integrals, an expression for Eq. (15) was found, for the case of an isotropic harmonic trap of frequency ω, in the form

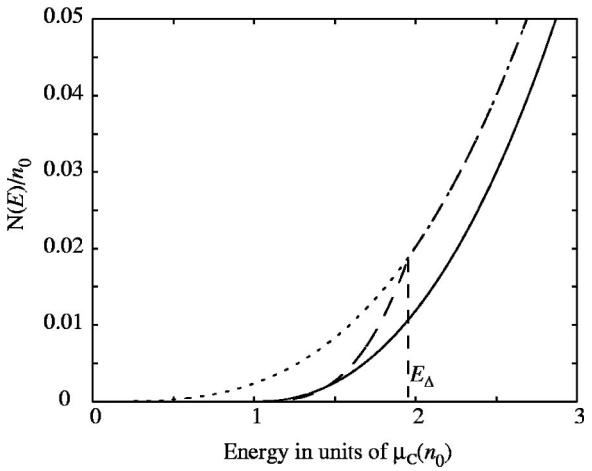

FIG. 4. The cumulative number of states N(E) below an energy E. The solid line shows the results obtained using the semiclassical approximation for the isotropic trap equation (16), and the dotted line shows the case for the noninteracting harmonic well. The dashed line represents the form used in this paper with $E_\Delta = 2\mu_C(n_0)$. The results were obtained for a condensate of 5 000 000 atoms at a temperature of 900 nK.

$$\frac{\mathrm{N}(\tilde{E})}{n_0} = \tilde{E}^2\sqrt{(1-x)(x+\eta/\tilde{E})} + \int_0^{\tilde{E}} d\tilde{\varepsilon}\frac{4}{\pi\zeta(3)}\int_0^1 dx\,\tilde{\varepsilon}\,\eta\sqrt{\frac{[x^2+\tilde{\varepsilon}^2/\eta^2]^{1/2}-x}{x^2+\tilde{\varepsilon}^2/\eta^2}}, \tag{16}$$

where

$$\eta = \frac{\mu_C(n_0)}{kT_c}, \quad kT_c = \hbar\omega\left(\frac{n_0}{\zeta(3)}\right)^{1/3}. \tag{17}$$

The chemical potential $\mu_C(n_0)$ is given by the Thomas-Fermi approximate form (12), and the energy is given in the dimensionless units $\tilde{E} = E/kT_c$. This semiclassical form for $N(E)$ was found in Refs. [16,15] to be practically indistinguishable from that found by numerical solutions of the Bogoliubov spectrum over the entire range of energies.

In Fig. 4 the semiclassical form of N(E) obtained from Eq. (16) is compared to that of the noninteracting harmonic oscillator [given by Eq. (11)], and the density of states obtained using our model with E_Δ equal to $2\mu_C(n_0)$. The figure does not show very good agreement of our model with the semiclassical results at moderate energies, although at low energies the agreement is good. At high enough energies (not shown) the noninteracting potential results become practically indistinguishable from those obtained from the semiclassical method, the energy at which this occurs is about $5\mu_C(n_0)$ for the results in Fig. 4. It should be emphasized that this semiclassical result applies to an isotropic trap, and the consideration of the anisotropy of realistic traps, which has not yet been accounted for, may have a significant effect on the spectrum.

4. Approximations

Several approximations that have been made in the derivation of this model rely on the condensate band being small relative to the noncondensate band, and if E_R and E_Δ are too large then these approximations will not be valid. The approximations concerned are the following.

(i) That the noncondensate band is so large that it is essentially undepleted by the process of condensate growth.

(ii) That the scattering processes between condensate band atoms may be taken as being negligible compared to the interband scattering processes, as will be assumed later.

It should be noted, and will be shown later, that the major effect on the overall growth due to mean-field effects is caused by the changes in energies of the lowest-energy levels, and for these levels the model proposed here is in quite good agreement with the semiclassical results. Because of this, as well as for the above reasons, the value of E_Δ used will generally remain equal to $2\mu_C(n_{0,f})$. The value of E_R is chosen somewhat larger. This provides a check that the solutions we find do match smoothly onto the distribution above E_R, which is assumed not to change.

D. Dynamical processes

The dynamics which will be considered in order to describe the evolution of the condensate band arise from the following processes.

(a) Two particles in the noncondensate band collide, one of the particles leaves with an increased energy, and the remaining particle enters the condensate band, now having an energy less than E_R. Of course the reverse process must also be considered—a noncondensate band particle colliding with a condensate band particle and exciting it out of the condensate band.

(b) A noncondensate band particle collides with a condensate band particle and exchanges energy such that both particles end up in the condensate band, and the reverse process.

(c) A noncondensate band particle collides with a condensate band particle, transferring some energy, but both particles remain in their respective bands.

(d) Two particles in the condensate band collide, transferring energy, with the result that both particles remain in the condensate band, but having different energies than before the collision.

Processes (c) and (d) will be termed *scattering processes*, since they do not change the occupation number of either band. Processes (a) and (b) cause the number of particles in the condensate band to increase, and so will be referred to as *growth processes*. The distinction between the two types of processes is illustrated in Fig. 5. Because the number of atoms in the noncondensate band is much larger than that in the condensate band, the scattering will be dominated by processes of type (c), and those of type (d) will be neglected.

These processes are described by the full quantum kinetic master equation obtained in QKIII and QKV, which can be used to determine rate equations for the evolution of the system.

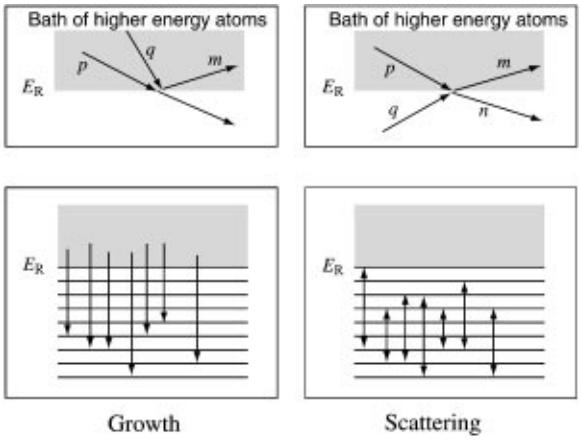

FIG. 5. Illustration of the two types of dynamical processes, growth and scattering. Only the two noncondensate particle growth process is shown [process (a) in the text], and only noncondensate–condensate band scattering is shown [process (c)].

E. Growth processes

The formalism of Refs. [17,12,14] gives rise to rate equations for N, the number of particles in the condensate band as a whole, and n_m, which represent the number of quasiparticles in the mth quasiparticle level. The derivation gives equations in the limit that N is sufficiently large for us to write $n_0 \approx N$. The rate equations take the form

$$\frac{dn_m}{dt} = \dot{n}_m|_{\text{growth}} + \dot{n}_m|_{\text{scatt}}. \tag{18}$$

The form of $\dot{n}_m|_{\text{growth}}$ was given in QKIII, Sec. IV E 3, and can be written in terms of the transition rates as

$$\dot{n}_m = \dot{n}_m^+ + \dot{n}_m^-, \tag{19}$$

$$\dot{N} = 2W^+[(1-e^{(\mu_C(N)-\mu)/k_BT})N+1] + \sum_m \{\dot{n}_m^+ - \dot{n}_m^-\}, \tag{20}$$

where

$$\dot{n}_m^+ \equiv 2W_m^{++}(N)[(1-e^{[\mu_C(N)-\mu+\epsilon_m]/k_BT})n_m+1], \tag{21}$$

$$\dot{n}_m^- \equiv 2W_m^{-+}(N)[(1-e^{[-\mu_C(N)+\mu+\epsilon_m]/k_BT})n_m+1]; \tag{22}$$

the relationships between forward and backward rates can be shown to be

$$W^+(N) = e^{[\mu-\mu_C(N)]/kT}W^-(N), \tag{23}$$

$$W_m^{++}(N) = e^{[\mu-\mu_C(N)-\epsilon_m]/k_BT}W_m^{--}(N), \tag{24}$$

$$W_m^{+-}(N) = e^{[\mu-\mu_C(N)+\epsilon_m]/k_BT}W_m^{-+}(N). \tag{25}$$

In these equations, the energies of the quasiparticle excitations ϵ_m are measured from the *ground-state energy*, which is $\mu_C(N)$.

1. Transitions

There are six processes which are described by these equations.

(i) $N \to N+1$, with no change in $\mathbf{n}$. The transition probability for this process is $W^+(N) = R^+(\xi_N, \mu_C(N)/\hbar)$.

(ii) $N \to N-1$, with no change in $\mathbf{n}$. The transition probability for this process is $W^-(N) = R^-(\xi_{N-1}, \mu_{N-1}/\hbar)$.

(iii) $N \to N+1$, with $n_m \to n_m+1$. The transition probability for this process is $W_m^{++}(N) = R^+[f_m, (\epsilon_N^m + \mu_C(N))/\hbar]$.

(iv) $N \to N-1$, with $n_m \to n_m-1$. The transition probability for this process is $W_m^{2--}(N) = R^-(f_m, (\epsilon_{N-1}^m + \mu_{N-1})/\hbar)$.

(v) $N \to N+1$, with $n_m \to n_m-1$. The transition probability for this process is $W_m^{+-}(N) = R^+(g_m, (-\epsilon_N^m + \mu_N)/\hbar)$.

(vi) $N \to N-1$, with $n_m \to n_m+1$. The transition probability for this process is $W_m^{-+}(N) = R^-(g_m, (-\epsilon_{N-1}^m + \mu_{N-1})/\hbar)$.

Here the functions f_m and g_m are amplitudes for the creation and destruction of atoms in quasiparticle states with energies ϵ_N^m, which are defined in Refs. [17,12], but whose explicit form will not need to be used here; ξ_N is the condensate wave function for N atoms. The functions $R^{\pm}(y,\omega')$ are defined by

$$R^+(y,\omega') = \frac{u^2}{(2\pi)^5\hbar^2}\int d^3\mathbf{r}\int d^3\mathbf{K}_1\, d^3\mathbf{K}_2\, d^3\mathbf{K}_3\, d^3\mathbf{k} \times \delta(\Delta\omega_{123}(\mathbf{r}) - \omega')\delta(\mathbf{K}_1+\mathbf{K}_2-\mathbf{K}_3-\mathbf{k}) \times F_1F_2(1+F_3)\mathcal{W}_y(\mathbf{r},\mathbf{k}), \tag{26}$$

$$R^-(y,\omega') = \frac{u^2}{(2\pi)^5\hbar^2}\int d^3\mathbf{r}\int d^3\mathbf{K}_1\, d^3\mathbf{K}_2\, d^3\mathbf{K}_3\, d^3\mathbf{k} \times \delta(\Delta\omega_{123}(\mathbf{r}) - \omega')\delta(\mathbf{K}_1+\mathbf{K}_2-\mathbf{K}_3-\mathbf{k}) \times (1+F_1)(1+F_2)F_3\mathcal{W}_y(\mathbf{r},\mathbf{k}). \tag{27}$$

In these equations the following notation is used:

$$\hbar\omega_{\mathbf{K}_i}(\mathbf{r}) \equiv \frac{\hbar^2\mathbf{K}_i^2}{2m} + V_T(\mathbf{r}), \tag{28}$$

$$\Delta\omega_{123} \equiv \omega_{\mathbf{K}_1} + \omega_{\mathbf{K}_2} - \omega_{\mathbf{K}_3}, \tag{29}$$

$$\Delta\mathbf{K} \equiv \mathbf{K}_1 + \mathbf{K}_2 - \mathbf{K}_3 - \mathbf{k}, \tag{30}$$

$$u = \frac{4\pi\hbar^2 a}{m}. \tag{31}$$

The function $F_i = F(\mathbf{K}_i, \mathbf{r})$ is the distribution function for the noncondensate particles, and the Wigner function is given by

$$\mathcal{W}_y(\mathbf{r},\mathbf{k}) = \frac{1}{(2\pi)^3}\int d^3\mathbf{v}\, y^*\left(\mathbf{r}+\frac{\mathbf{v}}{2}\right) y\left(\mathbf{r}-\frac{\mathbf{v}}{2}\right) e^{i\mathbf{k}\cdot\mathbf{v}}. \quad (32)$$

The R^+ function is related to collisions between two noncondensate band particles with momenta $\mathbf{K}_1$ and $\mathbf{K}_2$, from which the particles leave with momenta $\mathbf{K}_3$ and $\mathbf{k}$. The particle with momentum $\mathbf{k}$ is now in the condensate band (i.e., $\mathbf{k}$ is small) so that the particle with momentum $\mathbf{K}_3$ remains in the noncondensate band. The functions $R^{\pm}(y,\omega')$ therefore represent the rates for collisions which result in a particle entering $(+)$ or leaving $(-)$ the condensate band with an energy $\hbar\omega'$.

2. Approximate evaluation of transition rates

The rate factors $W^{\pm}(N)$ contain integrals over all space of terms containing the product of $F(\mathbf{K},\mathbf{r})$ terms times the Wigner function corresponding to the ground-state wave function $\mathcal{W}_{\xi_N}(\mathbf{r},\mathbf{K})$. In practice the ground-state wave function is very sharply peaked in comparison to the spatial dependence of the $F(\mathbf{K},\mathbf{r})$ functions which describe the remainder of the cloud of atoms. This means that in the spatial integral for the $W^{\pm}(\mathbf{r})$ terms [from Eqs. (26)] the $F(\mathbf{K},\mathbf{r})$ terms can be approximated by their values at $\mathbf{r}=0$. This gives

$$W^+(N) = \frac{u^2}{(2\pi)^5\hbar^2}\int d^3\mathbf{K}_1\int d^3\mathbf{K}_2\int d^3\mathbf{K}_3\int d^3\mathbf{k}\,\delta(\Delta\mathbf{K})\,\delta[\Delta\omega_{123}(\mathbf{0})-\mu_C(N)/\hbar]F(\mathbf{K}_1,\mathbf{0})F(\mathbf{K}_2,\mathbf{0})$$
$$\times[1+F(\mathbf{K}_3,\mathbf{0})]|\tilde{\xi}_N(\mathbf{k})|^2 \quad (33)$$

$$W^-(N+1) = \frac{u^2}{(2\pi)^5\hbar^2}\int d^3\mathbf{K}_1\int d^3\mathbf{K}_2\int d^3\mathbf{K}_3\int d^3\mathbf{k}\,\delta(\Delta\mathbf{K})\,\delta[\Delta\omega_{123}(\mathbf{0})-\mu_C(N)/\hbar][1+F(\mathbf{K}_1,\mathbf{0})]$$
$$\times[1+F(\mathbf{K}_2,\mathbf{0})]F(\mathbf{K}_3,\mathbf{0})|\tilde{\xi}_N(\mathbf{k})|^2, \quad (34)$$

in which $\tilde{\xi}_N(\mathbf{k})$ is the momentum-space ground-state wave function, obtained from the spatial form by

$$\tilde{\xi}_N(\mathbf{k}) = \frac{1}{(2\pi)^{3/2}}\int d^3\mathbf{r}\, e^{i\mathbf{k}\cdot\mathbf{r}}\xi_N(\mathbf{r}). \quad (35)$$

In Ref. [5], progress was made by assuming that the noncondensate band distribution $F(\mathbf{K},\mathbf{r})$ was given by the classical Maxwell-Boltzmann distribution

$$F(\mathbf{K},\mathbf{r}) \approx \exp\left(-\frac{\hbar^2\mathbf{K}^2/2m+V_T(\mathbf{r})-\mu}{kT}\right), \quad (36)$$

with values of T and μ which ensure the formation of a condensate once the system reaches equilibrium. Furthermore, in calculating the integrals in Eqs. (33) and (34), it was assumed that the range of condensate band energies was negligible compared to that of the noncondensate band. Thus the range of $\mathbf{k}$ was negligible compared to the range of $\mathbf{K}_{1,2,3}$, and the integrals in $\mathbf{K}_{1,2,3}$ were calculated over all energies rather than just over the noncondensate band. The function $F(\mathbf{K},\mathbf{r})$ was also assumed to be negligible compared to unity. The result obtained was [5]

$$W^+(N) = \frac{4m(akT)^2}{\pi\hbar^3}e^{2\mu/kT}\left[\frac{\mu_C(N)}{kT}K_1\left(\frac{\mu_C(N)}{kT}\right)\right]. \quad (37)$$

Here $K_1(x)$ is a modified Bessel function. In almost all practical situations the term in square brackets in the above equation is approximately equal to unity, and so W^+ is essentially independent of N. The value of $W^-(N)$, the rate of transitions out of the condensate band, can be obtained in a similar fashion to that for W^+. The ratio of forward to backward rates is found to be given by

$$W^+(N) = e^{(\mu-\mu_C(N))/kT}W^-(N), \quad (38)$$

which stems from the assumption of the thermal undepleted bath, and the definitions of W^+ and W^-. From this equation and the master equation it can be seen that equilibrium is achieved when $\mu_C(N)=\mu$ to order $1/N$.

3. Simple growth equation

A rate equation for the mean number of atoms in the condensate $\langle N\rangle$ (written as N for convenience for the rest of this section) was obtained in [5,12]

$$\dot{N} = 2W^+(N)\{(1-e^{(\mu_C(N)-\mu)/k_BT})N+1\}. \quad (39)$$

This equation is the *simple growth equation* used for the simulations of condensate growth in Refs. [5,12]. If the sys-

tem starts with $N=0$, the growth begins slowly (but at a finite rate). Once a significant condensate occupation is attained the term proportional to N becomes dominant, causing a much faster growth rate. The growth eventually slows as $\mu_C(N)$ approaches μ and the system settles into equilibrium. This gives the curve an S shape, as will be shown in the next section.

By using the Thomas-Fermi chemical potential [Eq. (12)] for $\mu_C(N)$, and the Maxwell-Boltzmann form for $W^{\pm}(N)$, the first simulations for the growth of a realistic condensate were presented in Ref. [5]. The growth equation is simple to solve numerically, for whatever number of particles is necessary (for example, the growth of a condensate containing 5 000 000 atoms was simulated in Ref. [5]).

4. Beyond the simple growth equation

The derivation of the simple growth equation contains a number of approximations and simplifications. The major behavior once N becomes large should be described quite well by the simple growth equation, but terms which were neglected may have significant effects during the initial stages of growth. Possibly significant factors which should first be considered are the following.

(i) The effect of considering all quasiparticle levels (the excited levels in the condensate band).

(ii) The effect of scattering processes (as defined in Sec. II D).

(iii) Corrections to the $W^{\pm}(N)$ terms to consider the more realistic Bose-Einstein distribution function.

(iv) The fluctuations around the mean number.

This paper aims to consider the effects of incorporating the first three of these factors into the growth equation. During the process of Bose-Einstein condensate formation, the spectrum of eigenvalues makes a transition from the unperturbed spectrum of trap levels to the case where the spectrum is strongly affected by the condensate in the ground state. The Bogoliubov spectrum of a condensed gas is valid in the case where the number of particles in the condensate, n_0, is so large that it is valid to write $n_0 \approx N$. Thus, during the initial stages of condensate formation, where this is not true, one must use another formalism. In this paper we will consider the situation in which the interaction between the particles is very weak, as is in practice the case. This means that we will be able to use the unperturbed spectrum for the initial stages of condensation, and only use the Bogoliubov description once enough condensate has formed to make the effective interaction rather stronger.

The basic formalism of Ref. [12] can still be carried out in this case, and the modification that is found is rather minor—essentially, we make the substitution $N \to n_0$ in the chemical potential and the $W^{+}(N), W^{++}(N)$ functions, and set $W_m^{-+} \to 0$, since this term comes from the mixing of creation and annihilation operators which arises from the Bogoliubov method.

By making these adjustments, and now grouping the levels into subbands of energy e_m [measured now from zero, rather than from $\mu_C(N)$ as was the case for ϵ_m], with each subband containing g_m levels, the equations of motion for the growth processes are now

$$\dot{n}_m|_{\text{growth}} = 2W_m^{++}(n_0)\{[1-e^{(e_m-\mu)/kT}]n_m + g_m\}, \quad (40)$$

$$\dot{n}_0|_{\text{growth}} = 2W^{+}(n_0)\{[1-e^{[\mu_C(n_0)-\mu]/kT}]n_0 + 1\}. \quad (41)$$

We will make the further—possibly rather drastic—simplification, and entirely neglect the effect of phononlike quasiparticles, which are known to comprise only a very small fraction of the levels normally occupied at the temperatures considered. Thus the excited states are now taken to be of a purely single-particle nature, and the condensate band is now described by the occupation number of the condensate level (the lowest energy level) n_0, and by the occupation numbers of each of the excited states n_m. In this case, Eqs. (40) and (67) become the same as Eqs. (18)–(25), and may therefore be used to represent the full condensate growth process.

The complete neglect of phononlike quasiparticles can be justified by noting that the lower of these represent shape oscillations of the condensate itself. Thus, although these quasiparticle levels could become quite highly occupied, this really amounts to growth into an oscillating condensate. Experimentally this does happen, but large quasiparticle oscillations amount to a rather small fractional change in condensate shape, which is not expected to make much difference to the overall growth.

5. Evaluation of transition probabilities

The value for the transition probability $W^{+}(N)$ found in the simple growth equation (39) was derived by making some rather sweeping assumptions, and as such Eq. (37) is really just an order of magnitude estimate. To obtain a more accurate value the full Bose-Einstein distribution must be used for $F(\mathbf{K},\mathbf{r})$ and the ranges of integration of the noncondensate functions must exclude the condensate band in which $F(\mathbf{K},\mathbf{r})$ would become very large. We then have, from Eq. (33),

$$W^{+}(n_0) = \frac{u^2}{(2\pi)^5\hbar^2}\int d^3\mathbf{r}\int_{E>E_R} d^3\mathbf{K}_1\int_{E>E_R} d^3\mathbf{K}_2\int_{E>E_R} d^3\mathbf{K}_3\int_{E<E_R} d^3\mathbf{k}\,\delta(\Delta\mathbf{K})\,\delta(\Delta\omega_{123}(\mathbf{r})-\mu_C(n_0)/\hbar)F(\mathbf{K}_1,\mathbf{r})$$
$$\times F(\mathbf{K}_2,\mathbf{r})(1+F(\mathbf{K}_3,\mathbf{r}))\mathcal{W}_{\xi_{n_0}}(\mathbf{r},\mathbf{k}), \quad (42)$$

with

$$F(\mathbf{K},\mathbf{r})=\left[\exp\left(\frac{(\hbar^2\mathbf{K}^2/2m+V_T(\mathbf{r})-\mu}{kT}\right)-1\right]^{-1} \tag{43}$$

$$=\sum_{s=1}^{\infty}\exp\left(-s\left[\frac{\hbar^2\mathbf{K}^2/2m+V_T(\mathbf{r})-\mu}{kT}\right]\right). \tag{44}$$

Again, we have to make the following approximations.

(i) That the spatial dependence can be neglected, so $F(\mathbf{K},\mathbf{r})\rightarrow F(\mathbf{K},\mathbf{0})$ and $\mathcal{W}_{\xi_N}(\mathbf{r},\mathbf{k})\rightarrow|\xi_N(\mathbf{k})|^2$.

(ii) That we can neglect the $\mathbf{k}$ dependence, except in ξ_N, so that the only $\mathbf{k}$ dependence left is removed by $\int d^3\mathbf{k}|\xi_N(\mathbf{k})|^2=1$. The integrals over $\mathbf{K}_1$, $\mathbf{K}_2$, and $\mathbf{K}_3$ can then be performed, to give a final form for $W^+(n_0)$, found by Davis [18], of

$$W^+(n_0)=\frac{1}{2}\left(\frac{k_BT}{\hbar\omega}\right)^2\left\{[\log(1-z)]^2+z^2\sum_{r=1}^{\infty}[z\,z(n_0)]^r[\Phi(z,1,r+1)]^2\right\}, \tag{45}$$

where

$$z=e^{(\mu-E_R/k_BT)},\quad z(n_0)=e^{\{[\mu_C(n_0)-E_R]\}/k_BT}. \tag{46}$$

The function Φ is the *Lerch transcendent* [19], defined by

$$\Phi(x,s,a)=\sum_{k=0}^{\infty}x^k/(a+k)^s. \tag{47}$$

This form of $W^+(n_0)$ gives values of about a factor of 3 greater than the previous form in Eq. (37), depending on the exact parameters of the system, and this gives a correspondingly faster growth than that in Ref. [5].

The values for $W_m^{++}(n_0)$ are more difficult to obtain. The $W_m^{++}(n_0)$ terms are the average of the W^{++} terms for all the individual levels in the subband. The W^{++} terms are given by similar overlap integrals as used for the W^+ terms, and for the lower-energy levels in the condensate band, the overlap of the wave function with the spatial distribution of a noncondensate band particle should be similar to that for the condensate level. Thus it is expected that the W^{++} terms should be of the same order of magnitude as $W^+(n_0)$. Progress can therefore be made by approximating $W_m^{++}(n_0)\approx W^+(n_0)$. The effect and validity of this approximation will be investigated in Sec. II F.

F. Scattering processes

Scattering processes in this paper also need to be included in the evolution of n_m. Scattering between two atoms in the noncondensate band does not have to be explicitly considered, since it has been dealt with in making the assumption that the noncondensate band is an equilibrated time-independent thermal bath. Furthermore, the scattering between two condensate band atoms will be neglected since, at any time, the number of atoms in the condensate band is small relative to the number in the noncondensate band. The dominant scattering processes, and the only ones which will be considered, are the scattering of atoms between levels in the condensate band, due to interactions with noncondensate band atoms (see Fig. 5). These stem from terms in the full master equation which involve two condensate field operators ϕ. These terms give rise to a master equation of the form, as shown in QKIII, Eq. (50d):

$$\begin{aligned}\dot{\rho}|_{\text{scatt}}=&\sum_{\substack{mk\\ \epsilon_k<\epsilon_m}}\gamma_{km}\overline{N}_{km}\{2X_{km}\rho X_{km}^\dagger-[X_{km}^\dagger X_{km},\rho]_+\}\\&+\sum_{\substack{mk\\ \epsilon_k>\epsilon_m}}\gamma_{km}(\overline{N}_{km}+1)\{2X_{km}\rho X_{km}^\dagger-[X_{km}^\dagger X_{km},\rho]_+\}\\&+\sum_{\substack{km\\ \epsilon_k=\epsilon_m}}\gamma_{km}\overline{M}_{km}\{2X_{km}\rho X_{km}^\dagger-[X_{km}^\dagger X_{km},\rho]_+\},\end{aligned} \tag{48}$$

which is equivalent to the master equation governing the scattering of particles by a heat bath [20].

Here the operators are defined by

$$X_{km}\equiv a_m^\dagger a_k, \tag{49}$$

where a_k is the destruction operator for an atom in state k with energy ϵ_k. As in Sec. II E, we treat all excitations as being particlelike. The rates of the processes are determined by the factors γ_{km}, and the factors $\overline{N}_{km}$ are defined by

$$\overline{N}_{km}\equiv\frac{1}{\exp\left(\frac{\epsilon_k-\epsilon_m}{kT}\right)-1}. \tag{50}$$

The last line in the master equation (48) represents scattering between degenerate energy levels, which will not have any contribution to the time dependence of n_m once the levels are grouped into subbands, and so can be ignored.

The corresponding rate equation for $n_k=\langle a_k^\dagger a_k\rangle$, the mean occupation of the kth level, can easily be found from the master equation. When levels are grouped into subbands with mean energy e_k, occupation n_k, and with g_k levels contained in the subbands, it becomes

$$\begin{aligned}\dot{n}_k|_{\text{scatt}}=&\sum_{\substack{m\\ e_k>e_m}}\gamma_{km}\{\overline{N}_{km}n_m(n_k+g_k)-(\overline{N}_{km}+1)(n_m+g_m)n_k\}\\&+\sum_{\substack{l\\ e_k<e_l}}\gamma_{lk}\{(\overline{N}_{lk}+1)n_l(n_k+g_k)-\overline{N}_{lk}(n_l+g_l)n_k\}.\end{aligned} \tag{51}$$

The transition rates γ_{km} now represent averages over all the individual level transition rates which transfer an atom from the k subband to the m subband. The transition probabilities γ_{km} can be found in a similar manner to the $W^+(n_0)$ terms, from terms of the form [12]

$$R_{km}(N)=\frac{4u^2}{(2\pi)^5\hbar^2}\int d^3\mathbf{r}\int d^3\mathbf{K}_1\int d^3\mathbf{K}_2\int d^3\mathbf{k}\int d^3\mathbf{k}'\,\delta(\mathbf{K}_1-\mathbf{K}_2-\mathbf{k}+\mathbf{k}')F(\mathbf{K}_1,\mathbf{r})(1+F(\mathbf{K}_2,\mathbf{r}))$$
$$\times\mathcal{W}_k(N,\mathbf{r},\mathbf{k})\mathcal{W}_m(N,\mathbf{r},\mathbf{k}')\,\delta(\Delta\omega_{12}(\mathbf{r})-\Omega_m+\Omega_k), \tag{52}$$

where

$$\Omega_m(N)=\frac{\mu_C(N)+\epsilon_m(N)}{\hbar} \tag{53}$$

$$=\frac{e_m(N)}{\hbar}, \tag{54}$$

and the rest of the notation is as was used in Sec. II E.

1. Estimates for γ_{km}

Explicit computation involved in calculating these factors is impractical, and, it will turn out, unnecessary when the scattering is sufficiently strong. We shall instead estimate these γ_{km} rates by using the quantum Boltzmann approach of Holland *et al.* [21].

By treating the excitation spectrum as given by the eigenstates of the trapping potential, without modification by the presence of the condensate, and by using the ergodic assumption, Holland *et al.* obtained the kinetic equation [Eq. (12) in Ref. [21]]

$$g_n\frac{\partial f_n}{\partial\tau}=\sum_{mqp}\delta_{e_n+e_m,e_p+e_q}g(e_m,e_n,e_p,e_q)$$
$$\times[f_qf_p(1+f_m)(1+f_n)-(1+f_q)(1+f_p)f_mf_n], \tag{55}$$

in which $\tau=(8ma^2\omega^2/\pi\hbar)t$. The population of a level with energy e_n is f_n, and the degeneracy of levels at that energy is g_n. The collision kernel $g(e_m,e_n,e_p,e_q)$ is given from the overlap integrals for the states m, n, q, and p. However, when the energies of the levels considered are spread quite far apart, Holland *et al.* found from numerical calculations that the collision kernel $g(e_{\min},e_n,e_p,e_q)$ is well approximated by the degeneracy $g_{e_{\min}}$. Here $e_{\min}$ is the smallest of the energies in the collision. In our model the energies will always be quite well spread, as (a) they must be in different subbands, each subband being quite well separated from the next in terms of mean energy; and (b) the scattering processes we are attempting to describe must have e_m and e_p in the noncondensate band and e_q and e_p in the condensate band. Thus in our model we may safely use $g(e_{\min},e_n,e_p,e_q)\approx g_{e_{\min}}$.

By summing over m and p terms (which are levels higher than E_R), the effect of all the noncondensate (''bath'') levels on the condensate band atoms may be calculated. The kinetic equation for the scattering now becomes

$$\left.\frac{\partial n_n}{\partial\tau}\right|_{\text{scatt}}=\sum_q\left[(1+f_n)f_q\left(\sum_{mp}\delta(n,m;p,q)g_{e_{\min}}f_p(1+f_m)\right)\right.$$
$$\left.-(1+f_q)f_n\left(\sum_{mp}\delta(n,m;p,q)g_{e_{\min}}f_m(1+f_p)\right)\right], \tag{56}$$

where the following notation has been used:

$$n_m=f_mg_m, \tag{57}$$

$$\delta(n,m;p,q)\equiv\delta_{e_n+e_m,e_p+e_q}. \tag{58}$$

The terms of this equation can be simplified for the different possible cases.

First line, case $e_n>e_q$: In this case, $e_q=e_{\min}$, and energy conservation is satisfied when

$$e_p=e_m+\hbar\omega_{nq}, \tag{59}$$

where $\hbar\omega_{nq}=e_n-e_q$. The summation term in the first line of Eq. (56) then becomes

$$g_q\sum_{e_m>E_R}(1+f_m)f_{m+\omega_{nq}}\approx g_qe^{(\mu-\hbar\omega_{nq})/kT}\Gamma(T) \tag{60}$$

where

$$\Gamma(T)\equiv\sum_{e_m>E_R}e^{-e_m/kT}. \tag{61}$$

The approximation which has been made is that $(1+f_m)\approx1$, which should be acceptable since state m is of high energy (i.e., in the noncondensate band). The calculation of $\Gamma(T)$ requires a knowledge of the spectrum of energies in the noncondensate band, which is complicated for an anisotropic trap. The form for an *isotropic* harmonic potential $\bar{\Gamma}(T)$ is easily calculated though, and gives

$$\bar{\Gamma}(T)=\frac{e^{-E_R/kT}}{1-e^{-\hbar\omega/kT}}, \tag{62}$$

where ω is the frequency of the potential. We will therefore make the approximation that $\Gamma(T)\approx\bar{\Gamma}(T)$ for the determination of γ_{km}, using the geometrical mean frequency of the real trap as the frequency of the isotropic potential. Thus $\omega=(\omega_x\omega_y\omega_z)^{1/3}$ in Eq. (62).

Remaining terms: Similar reasoning leads to the results

$$g_n \sum_{e_p > E_R} (1+f_{p+\hbar\omega_{qn}}) f_p \approx g_n \sum_{e_p > E_R} e^{(\mu - e_p)/kT} \tag{63}$$

$$= g_n e^{\mu/kT} \Gamma(T), \tag{64}$$

$$g_q \sum_{e_m > E_R} f_m (1+f_{m+\hbar\omega_{nq}}) \approx g_q e^{\mu/kT} \Gamma(T,R), \tag{65}$$

$$g_n \sum_{e_p > E_R} f_{p+\hbar\omega_{qn}} (1+f_p) \approx g_n e^{(\mu-\hbar\omega_{qn})/kT} \Gamma(T). \tag{66}$$

2. Total scattering equation

The total kinetic equation governing the scattering processes is now given by

$$\dot{n}_m|_{\text{scatt}} = \frac{8ma^2\omega^2}{\pi\hbar} e^{\mu/k_B T} \Gamma(T) \times \left\{ \sum_{k<m} \frac{1}{g_m} [n_k(g_m+n_m) e^{-\hbar\omega_{mk}/k_B T} - n_m(g_k+n_k)] + \sum_{k>m} \frac{1}{g_k} [n_k(g_m+n_m) - n_m(g_k+n_k) e^{-\hbar\omega_{km}/k_B T}] \right\}. \tag{67}$$

The notation $k>m$ is now being used to mean $e_k > e_m$. This is the rate equation governing scattering processes, it is equivalent to Eq. (51) if the following transformations are made:

$$\overline{N}(\omega_{nq}) \to e^{-\hbar\omega_{nq}/kT}, \tag{68}$$

$$1+\overline{N}(\omega_{nq}) \to 1, \tag{69}$$

$$\gamma_{nq} \to \frac{8ma^2\omega^2}{\pi\hbar} \frac{e^{\mu/kT}\Gamma(T)}{g_n} \quad \text{when} \quad n>q, \tag{70}$$

$$\gamma_{nq} \to \frac{8ma^2\omega^2}{\pi\hbar} \frac{e^{\mu/kT}\Gamma(T)}{g_q} \quad \text{when} \quad n<q. \tag{71}$$

G. Rate equations including scattering and growth

The total rate equation governing the evolution of this system is then given by adding Eq. (40) to Eq. (67),

$$\dot{n}_m = \dot{n}_m|_{\text{growth}} + \dot{n}_m|_{\text{scatt}}, \tag{72}$$

and for the condensate level evolution (41) is used in place of Eq. (40). It is useful here to review the major approximations that have been made in order to derive these equations. It was assumed that:

(i) the noncondensate band is very large, so it is essentially undepleted, and it is in equilibrium;

(ii) the influence of collective excitations is negligibly small, so that the states in the condensate band are all of single-particle nature;

(iii) the density of states in the system is as described in Sec. II C;

(iv) the ergodic approximation is valid, and that states in the condensate band which have similar energies may be ''binned'' together for the purpose of describing their evolution;

(v) the fluctuations of the occupation numbers around the mean numbers may be ignored;

(vi) the rate constants W^{++} for the growth processes which change the occupations of the excited states in the condensate band are equal to the rate constant for the growth of the condensate level;

(vii) the rate constant for the scattering processes in an anisotropic well of geometrical mean frequency ω is equal to that in an isotropic well with frequency ω;

(viii) three-body collisional processes may be ignored.

III. NUMERICAL SOLUTIONS OF THE GROWTH

The rate equations derived to describe the growth of a condensate in Sec. II are quite straightforward to solve numerically, and the solutions can be obtained in a matter of a few seconds as opposed to other numerical solutions which have been very time consuming. The nature of these solutions will be discussed and comparisons will be made with experimental data published in Ref. [4]. The parameters of the system modeled were chosen to be the same as in the MIT growth experiments:

(i) Using a dilute gas of ^{23}Na atoms, characterized by an *s*-wave scattering length of $a=2.75$ nm [22,4].

(ii) With an axially symmetric (''cigar shaped'') harmonic trapping potential described by the frequencies $\omega_x = \omega_y = 2\pi \times 82.3$ Hz and $\omega_z = 2\pi \times 18$ Hz, and giving a geometrical mean frequency of $\omega = 2\pi \times 50$ Hz [4,23].

(iii) With a total number of atoms of the order of 10^7, the numbers found in the condensate level once equilibrium is reached are in the range 5×10^5 to 1×10^7, giving a condensate occupation of between 5 and 30% of the total number of atoms [4,23]. In the majority of cases the thermal bath was therefore depleted by only a small amount, and the undepleted model which is used here should be a good approximation.

(iv) With temperatures in the range 0.5–1.5 μK [4,23].

A. Results

1. Simple growth equation results

Numerical solutions of the simple growth equation

$$\dot{n}_0 = 2W^+(n_0)\{(1-e^{(\mu_C(n_0)-\mu)/k_B T}) n_0 + 1\}, \tag{73}$$

are easily obtained [5], and an example of the resulting growth curve is shown in Fig. 6. This curve shows a characteristic S shape, the slow initial growth occurs as a result of spontaneous $(+1)$ terms in Eq. (73) and then, once the occupation becomes large enough, the stimulated growth terms (those proportional to n_0) dominate and the growth accelerates. The condensate grows quickly, until it approaches equilibrium where it slows again as $\mu_C(n_0)$ approaches μ, giving the final part of the S-shape nature.

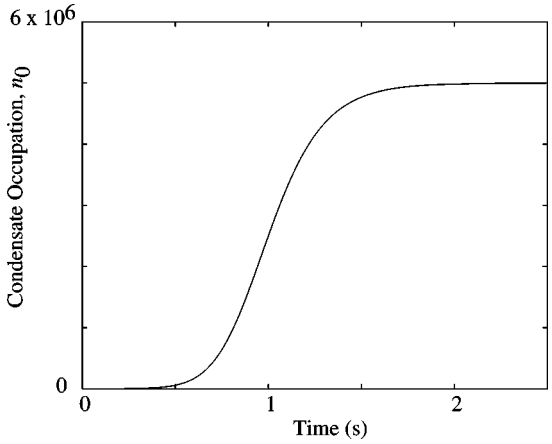

FIG. 6. Typical results of the simple growth equation for the growth of a Bose-Einstein condensate in the MIT apparatus at a temperature of 900 nK with $\mu = 43.3\hbar\omega$. The initial condensate occupation was taken to be 100 atoms.

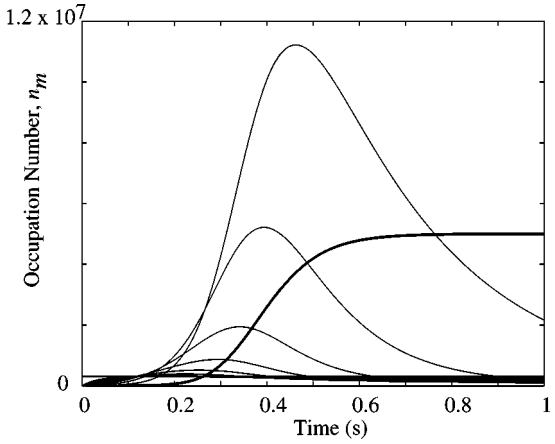

FIG. 7. Typical results of the new growth equations for the growth of a Bose-Einstein condensate using the same parameters as in Fig. 6. The condensate level (bold) reaches the equilibrium population of 5×10^6 atoms, the other lines represent the evolution of the populations of the other subbands in the condensate band. Note the much faster growth than in Fig. 6.

The derivation of the simple growth equation contained a number of significant approximations and assumptions. In effect it describes the situation in which the occupations of all levels higher in energy than the ground state are treated as time independent, giving an undepleted thermal bath in contact with only the condensate level. Furthermore, the populations of the levels in this bath are given by the Maxwell-Boltzmann distribution, rather than the correct Bose-Einstein distribution, and no mean-field effects are introduced. The simple growth equation is therefore just a first approximation for the growth, and was merely intended to give an order of magnitude description of the growth process. Indeed, as shall be shown in a subsequent section, experimental measurements [4] have shown that, although it gives the correct order of magnitude for time scale of the growth, the simple growth equation does not describe the rate of growth to any closer than a factor of about 3.

2. New model of growth processes

In order to improve the description of the growth over that of the simple growth equation, the first improvement which will be made is the more accurate calculation of W^+, using the full Bose-Einstein distribution. However, for lower-energy levels the equilibrium populations determined by the Bose-Einstein distribution are very large. Having such large populations in these levels will obviously not be a good model of a system rapidly cooled from a point where μ was negative to a region where μ has become positive, since the changes in populations of these levels required during this process are so substantial that a fairly long time will be required for the levels to come to equilibrium. It is therefore unphysical to consider a situation where the low-energy levels have reached their equilibrium populations before the condensate level has even started to evolve. For these reasons, it is not consistent to simply use the Bose-Einstein distribution to find W^+ in the model considered by the simple growth equation.

In order to develop a consistent description there need to be a number of lower-energy levels with time-dependent populations considered, forming the condensate band. Furthermore, the energies of these levels will be increased by the growth of the condensate, due to increased mean-field interactions. To describe this situation the model described in Sec. II must be implemented. Considering at first only the ''growth'' processes, the evolution was found in Sec. II E 4 to be given by

$$\dot{n}_m|_{\text{growth}} = 2W_m^{++}(n_0)\{[1-e^{(e_m-\mu)/kT}]n_m + g_m\}, \quad (74)$$

$$\dot{n}_0|_{\text{growth}} = 2W^{+}(n_0)\{[1-e^{[\mu_C(n_0)-\mu]/kT}]n_0 + 1\}, \quad (75)$$

where, for reasons given in Sec. II, we approximate $W_m^{++}(n_0)$ by $W^+(n_0)$. This form of evolution is essentially the simple growth equation applied to several energy levels.

It is now possible to perform a more accurate calculation of W^+, using the Bose-Einstein distribution to describe the population of levels above E_R (i.e., in the noncondensate band), and summing only over the noncondensate band levels. The new form of W^+ is given by Eq. (45).

Sample solutions to the coupled differential equations (74) and (75) are shown in Fig. 7. The rate of growth of the condensate has increased substantially (generally by at least a factor of 3) over that predicted by the simple growth equation, this is due to the more accurate calculation of $W^+(n_0)$. However, the shape of the growth is still essentially the same as that given by the simple growth equation.

It can be seen from Fig. 7 that the lower-energy levels also experience very substantial growth in this model. Indeed the occupations of some of these levels can exceed the condensate occupation substantially before relaxing back to their equilibrium values. This is of course not a realistic scenario, and is certainly not one that has been observed in any experiments. Note that the number of subbands used in this figure (and most of the other figures presented) is substantially fewer than would normally be used. Generally the number of subbands required is about 20–50, depending on

the exact parameters; however, these cannot be well distinguished from each other in a graph. Therefore, throughout this paper, most of the depictions of the growth of subbands will show only a few of them.

Once scattering processes are included (see below), reducing the number of subbands used causes the growth to become slower. It also causes the model to become less realistic, since an individual level may then be described by an average energy quite different from its actual energy. If the number of subbands is increased, an asymptotic limit to the speed of the growth is reached, however this is also unrealistic since now some subbands contain only fractions of individual energy levels. The choice used in practice is such that in their final equilibrium states the subbands have widths of $\hbar\omega$. This choice is close to the asymptotic limit, and ensures at least three individual levels are contained in the first subband.

3. Inclusion of scattering processes

If we include scattering processes, as given by Eq. (67), the picture is dramatically changed. Solutions for the resulting evolution equations (72) are shown in Fig. 8. This figure shows that the scattering has two main effects. First, the initiation of the condensate level growth occurs much more sharply, this gives a substantial change to the shape of the growth, which has now lost much of the S-shape nature that previous solutions had shown. The speed of the growth after the initiation is changed little by the inclusion of the scattering processes, since in this region growth is completely dominated by the growth processes. The second effect is that the populations of the excited states no longer exceed plausible levels.

The reasons behind these changes are interlinked. Without scattering, all of the levels in the condensate band start to grow, and at quite similar rates. The difference in the growth rate between the very low energy states and that of the condensate level is particularly small. Because of the degeneracy of states in the lower subbands a large population can form in them, which can become very much larger than the condensate level population. Once any one subband acquires a sufficient population, the stimulated term in the growth process begins to dominate, and the population increases even further. In the absence of scattering processes, the only way in which the excess population in these states can be transferred to the condensate level, where it will be found in the equilibrium situation, is by a transfer back to the noncondensate band followed by another collision which transfers it directly to the condensate level.

If scattering processes are considered, atoms may now be transferred directly between different levels in the condensate band in a collision. Any excess population in the excited states can then be quickly transferred out of the state before the stimulated growth process becomes too dominant.

With the inclusion of the scattering processes, the effects of two important approximations must be considered. In the derivation of the equations governing the scattering processes it was assumed that the value of $\Gamma(T)$

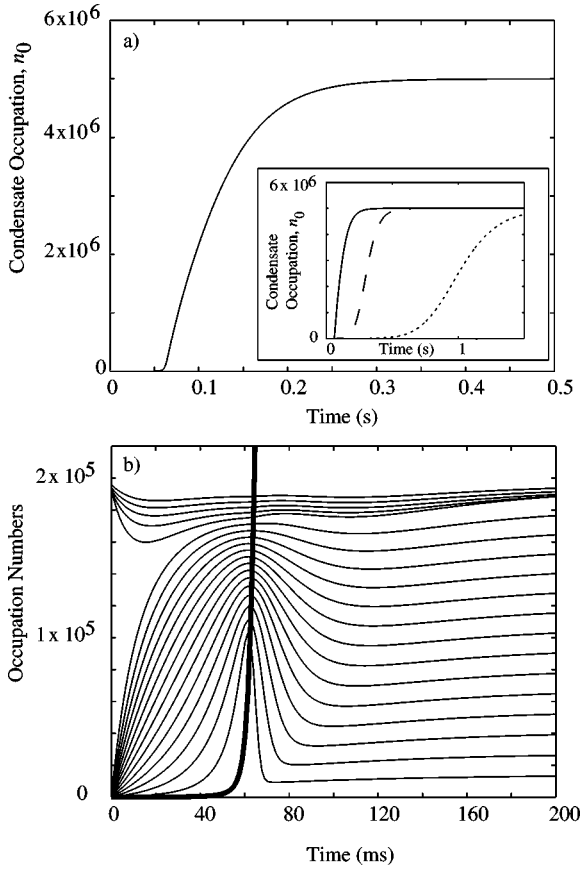

FIG. 8. Typical results of the total growth equation (including scattering processes) for the growth of a Bose-Einstein condensate using the same parameters as in Fig. 6. (a) The growth of the condensate (ground state) occupation. The inset shows the same growth predicted by the total new model (solid line) compared to the growth predicted without considering scattering processes (dashed line), and that of the simple growth equation with an initial population of 100 atoms (dotted line). (b) The growth of the explicitly considered subbands. The condensate level itself is the bold curve. The top five subbands are those in the noncondensate band which were explicitly considered. Note the different time scales on the graphs.

$\equiv\Sigma_{e_m>E_R}e^{-e_m/kT}$ was equivalent to that for an isotropic harmonic oscillator $\overline{\Gamma}(T)$, which affects the scattering rates.

The second important approximation was made in the solution of the equations governing the growth processes, where the $W_m^{++}(n_0)$ terms were assumed to be equal to $W^{+}(n_0)$, which has a value given by Eq. (45). This approximation has no effect on the growth rate of the condensate level if the scattering terms are not considered, since then there are no interactions between different levels in the condensate band. The effects of these two approximations are discussed below.

4. Effect of the scattering rate approximation

The magnitude of the scattering rate was assumed to be equal to that for an isotropic harmonic oscillator in the derivation of Eq. (67). In Fig. 9, the growth of the condensate

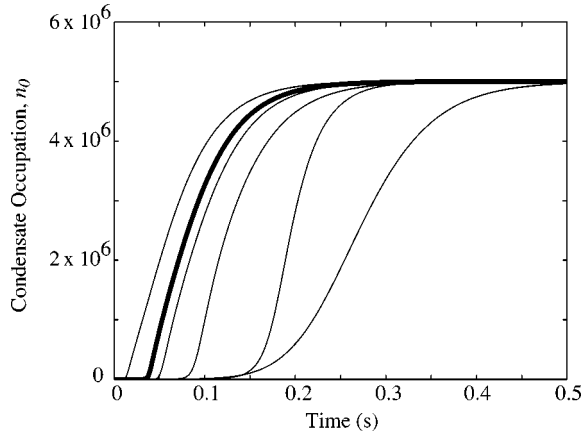

FIG. 9. The dependence on the rate for scattering processes of the condensate level growth. Growth curves from left to right had factors $\Gamma(T)$ of $100\Gamma(T)$, $\Gamma(T)$, $\Gamma(T)/2$, $\Gamma(T)/10$, $\Gamma(T)/100$, and zero, respectively, where $\Gamma(T)$ is the factor for the isotropic harmonic potential given by equation (62). These results were obtained using the same parameters as used in Fig. 8.

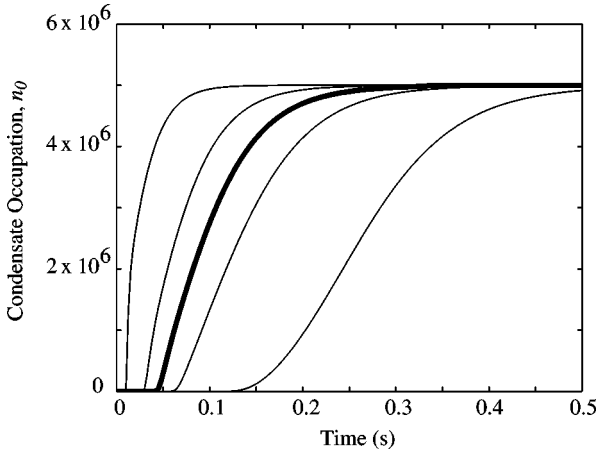

FIG. 10. The effect on the rate of growth of the condensate when the values of $W_m^{++}(n_0)$ were changed. From left to right the curves correspond to values for $W_m^{++}(n_0)$ of $10W^+(n_0)$, $2W^+(n_0)$, $W^+(n_0)$, $W^+(n_0)/2$, and $W^+(n_0)/10$. Conditions correspond to those in Fig. 8.

level is shown for several different scattering rates. The growth slows slightly if the rate is decreased. If the rate is increased, the growth becomes faster until it reaches an asymptotic limit at which point it is the rate of the growth processes which determines the speed of growth. The results show that the overall growth changes by only a relatively small amount (and certainly smaller than present experimental uncertainties in growth experiments), provided that the rate is within two orders of magnitude of that for the isotropic trap. Since it seems unlikely that the corrections due to the anisotropy would change the rate by much more than one order of magnitude, the approximation of using the isotropic rate factor seems to be valid. It is interesting to note that a scattering rate of only about 1% of the isotropic case is usually sufficient to prevent the occupations of the subbands becoming very large as they do in the absence of any scattering.

5. Effect of W_m^{++} factors

The effect of the approximation $W_m^{++}(n_0) \approx W^+(n_0)$ is shown in Fig. 10 which shows the behavior of the growth for different values of the $W_m^{++}(n_0)$ terms. Changing $W_m^{++}(n_0)$ changes the rate of growth of the excited states, and thus changes the probability of atoms being scattered from the excited states into the condensate level, giving a corresponding change in the overall growth of the condensate. The results show that provided $W_m^{++}(n_0)$ lies in the range $2W^+(n_0) > W_m^{++}(n_0) > W^+(n_0)/2$ then the growth rate does not change significantly (compared to experimental uncertainties and the change caused by using an accurate scattering rate). However, outside of this range the growth is altered considerably. The expectation is that $W_m^{++}(n_0)$ will lie in the desired range, since it is an average over quantities similar to $W^+(n_0)$, and as such should be of the same magnitude. The ''standard'' approximations for the rate constants that will be used in the following results will be $W_m^{++}(n_0) = W^+(n_0)$ and $\Gamma(T) = \bar{\Gamma}(T)$.

6. Initial conditions

A problem which has to be considered in solving the total rate equations (72) is the determination of the correct initial conditions. Because the noncondensate band is assumed to be a thermal bath of atoms at equilibrium, the initial populations for the explicitly considered levels in this band are found from $[\exp((E-\mu)/kT)-1]^{-1}$. Obviously this cannot be used to give the initial populations in the condensate band when the model is attempting to describe growth of the condensate. It is not immediately obvious what the appropriate initial conditions should be for the condensate band. In Fig. 11, four different initial conditions are shown:

(a) No initial population in the condensate band. This is the most artificial of the four possibilities presented.

(b) Initial population of zero in the condensate level and excited-state occupations given by a linear dependence on energy rising to match that of the noncondensate band at E_R.

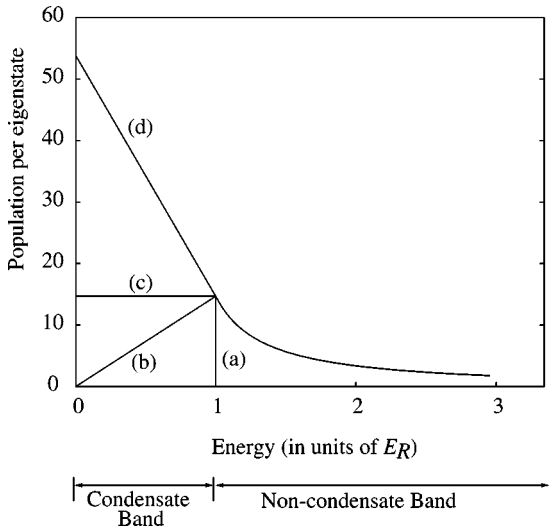

FIG. 11. Depiction of the four different initial populations trialed, as described in the text.

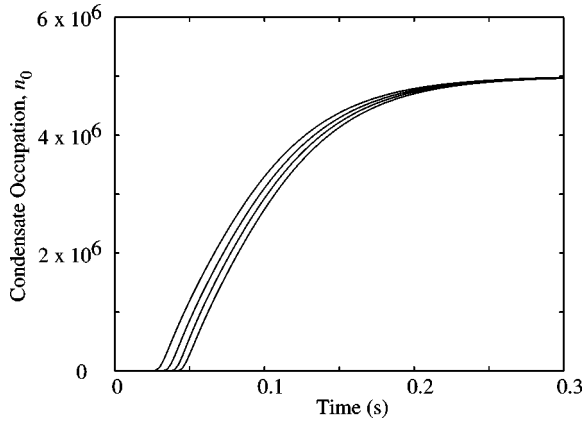

FIG. 12. Growth curves determined using the initial conditions described in the text. The curves, from slowest to fastest growth, were given by initial conditions (a)–(d) respectively. Conditions are the same as for Fig. 8.

(c) Initial populations of condensate band states all equal to the value of $[\exp((E_R-\mu)/kT)-1]^{-1}$.

(d) Initial populations given by a linear extrapolation of the noncondensate populations, meeting $[\exp((E-\mu)/kT)-1]^{-1}$ tangentially at E_R.

In Fig. 12 the growth curves corresponding to each of the differing initial conditions are shown. The different initial conditions can be seen to have little effect on the shape of the growth; the main effect is really just a small shift in the initiation time. This effect is generally quite small compared to the effects of changing $\Gamma(T)$ and $W_m^{++}(n_0)$, as seen in the preceding sections. The fact that the initial conditions can be changed by so much and yet have little effect on the growth curve is due mainly to the inclusion of the scattering terms. The scattering terms very quickly cause the levels in the condensate band to come to a kind of quasiequilibrium from whatever initial state they are put in. Thus we conclude that an exact knowledge of the initial conditions is not important.

Since the exact initial conditions do not seem to be important, in all further calculations initial condition (c) will be used, as it is about midway between the extremes of cases (a) and (d).

7. Modifications of the energies of the subbands

The previous results were all obtained by taking the mean-field effects due to the condensate into account in the manner described in Sec. III A 6. That is to evenly distribute the energies of the subbands between the fixed upper limit of E_Δ and the n_0-dependent lower limit $\mu_C(n_0)$. Thus all levels below E_Δ [fixed at $2\mu_C(n_{0,f})$, where $n_{0,f}$ is the final occupation of the condensate level] are modified at all times. This artificial model can be improved on, since the number of levels affected by the condensate depends upon its occupation. In other words, when there is only a small condensate present it has a significant effect on only the lower subbands, while the upper subbands are essentially unmodified. An improved (although still a little artificial) method is the following: all levels below $\gamma\mu_C(n_0)$ (where γ is an arbitrary parameter) will be compressed to fit between this upper limit

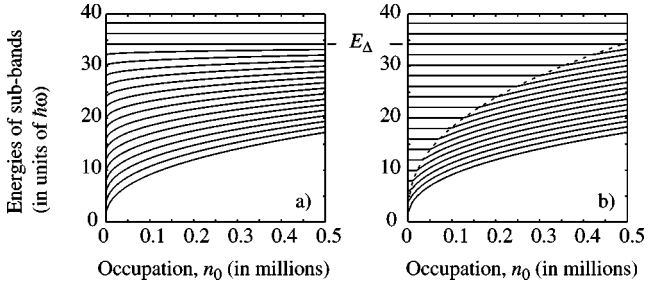

FIG. 13. The energy spectrum of the subbands as a function of n_0, modified to account for the mean-field interactions with the growing condensate. In (a) the levels are modified by changing all levels in the condensate band, as has been used to obtain the previous results. In (b) these effects are accounted for by the new model, explained in the text. The lowest-energy level is the condensate level, whose energy is $\mu_C(n_0)$. The dotted line represents $2\mu_C(n_0)$, the maximum energy at which mean-field corrections are assumed to be significant. This figure shows the evolution of the energies for a temperature of 900 nK, and with a final (equilibrium) condensate occupation of 5×10^5. The few levels whose energies never change are those levels in the noncondensate band (above E_R) which are explicitly considered.

and the lower limit of $\mu_C(n_0)$; the energies of all levels higher than $\gamma\mu_C(n_0)$ will not be altered. This is similar to the previous model, with the alteration that the upper limit of the levels whose energies are changed is no longer fixed, but instead rises with increasing n_0. The energy of a level e_m is then given by

$$e_m=\begin{cases} e_m^0 & \text{for } e_m^0>\gamma\mu_C(n_0) \\ \mu_C(n_0)+e_m^0\left(1-\dfrac{1}{\gamma}\right) & \text{for } e_m^0<\gamma\mu_C(n_0), \end{cases} \tag{76}$$

where e_m^0 are the unchanged energy levels, as given by the eigenstates for a noninteracting gas in a harmonic potential. The energy spectrum of the subbands given by this new model is shown in Fig. 13, and compared to the previous energy spectrum. In the older model used so far in this paper all energy levels in the condensate band are changed by the growth of the condensate. However, the extent of the condensate band is determined by the final occupation number of the condensate [i.e., by the final value of $\mu_C(n_0)$]. In the new model, the levels are modified in a more consistent fashion, the energy levels for any given condensate population are determined by the condensate population at that time, which appears to be a more logical approach.

In Sec. II C 2 it was shown that a fair estimate for E_R was a value of $2\mu_C(n_{0,f})$. The value for γ will normally be taken to be 2, so that at equilibrium all energy levels below E_R will be modified.

The effect of this new model, compared to the earlier approach, on the overall growth is very small, smaller in fact than any of the other effects discussed in this section, and it is barely discernible. This would seem to indicate that it is the mean-field effects on the energies of the lower few subbands which are important when considering the growth of the condensate, since in both the old and new models the

lower levels experience quite similar changes. Since the mean-field effects of the condensate on the higher levels seems to have only a very small effect, the precise value of E_R would appear to have little effect so long as it is reasonably high. The value of $2\mu_C(n_{0,f})$ seems to be a good value, since it is high enough that the energy perturbations of higher energies do not have a large effect on the growth, and it is low enough that the majority of atoms are found at higher energies, giving an undepleted thermal bath.

B. Comparison of results with experiment

At the present point in time there has only been one published experiment which has investigated in any detail the growth of a Bose-Einstein condensate. The experiment was performed at MIT using a trapped gas of ^{23}Na atoms, and the results were published in 1998 in Ref. [4].

1. MIT experimental method

The MIT experiments were performed in the following way: The gas of atoms was confined in an approximately harmonic magnetic trap. It was then cooled using laser cooling and evaporative cooling techniques to a temperature slightly higher than the critical temperature necessary for the formation of a Bose-Einstein condensate. At this point the system is essentially in thermodynamic equilibrium, and then it is suddenly put into a nonequilibrium configuration of lower energy, by means of a rapid evaporative cooling ''cut'' which removes all atoms in states above a certain energy in a time of about 10 ms. The system is then left to relax to equilibrium with no further cooling. The cut will have brought the temperature of the gas below the critical temperature and so, to reach equilibrium, a condensate will form. The formation of the condensate is observed at several stages during the evolution by the means of phase-contrast microscopy.

This method attempts to achieve, probably as closely as is realistically possible, an almost thermalized bath in contact with a condensate band, as has been assumed in our theoretical treatment. The cut which removes the higher-energy atoms causes the wings of the energy distribution to be truncated. Experience with solutions of the quantum Boltzmann equation and related methods [24,21,11] shows that the effect of this will first be ''felt'' by the higher-energy atoms remaining. The higher levels will therefore be expected to thermalize more quickly, with thermalization gradually moving through to the lower energies. Thus at some point after the cut the majority of the atoms will be approximately in equilibrium, with the lower-energy atoms still in very nonequilibrium states.

2. MIT Experimental results and theoretical comparisons

Phase-contrast microscopy produces two dimensional images of the system with an intensity proportional to the column density of the system. From data of this type temperatures, total numbers of atoms, and condensate level occupations were extracted by the MIT group, and were presented in Ref. [4].

The results found in Ref. [4] were that condensate growth took on the order of 100–200 ms depending on the exact conditions. It was found that the growth could be well fitted by a solution of the simple growth equation (73), which can be put in the approximate (but in practice very accurate) form

$$\dot{n}_0 = \kappa_1 n_0 [1 - (n_0/n_{0,f})^{2/5}], \tag{77}$$

where, again, $n_{0,f}$ is the equilibrium condensate population. The solutions to this equation exhibit the S-shaped growth profile of Fig. 6.

The conclusion drawn in Ref. [4] was that a curve of this shape was evidence for the importance of bosonic stimulation in the growth processes, since a purely relaxational process would be described by solutions of

$$\dot{n}_0 = \kappa_2 (n_{0,f} - n_0). \tag{78}$$

However, the rate constants κ_1 found by the MIT group by fitting to the data obtained did not agree to better than an order of magnitude with the predictions of the simple growth equation of

$$\kappa_1 = 2W^+(n_0)\frac{\mu}{kT}. \tag{79}$$

The simple growth equation did well to give the correct order of magnitude rates; however, most of the predicted rates for higher temperatures seemed to be too small by about factor of 3. As the temperature decreased the discrepancy increased, the predicted rates became slower, while the experimentally fitted rate constants became larger.

In contrast, the solutions to the growth model presented in this paper no longer show the S shape, but are in fact closer in shape to the solutions of Eq. (78). These curves were found by MIT to describe the data quite poorly if the growth started at time $t=0$ (the time at which the cut finished). However, if an initiation time was allowed before the growth began, such solutions became quite close fits, although they still did not describe the initially slow growth giving the S shape to the growth. The results obtained in this paper show that, while the general shape is that of solutions to Eq. (78), there is also an initiation time present before the growth begins.

As a specific comparison with experiment, Fig. 14 shows the comparison between the growth curve predicted here and the experimental data. The data are similar to those in Ref. [4], but were not actually published. They were provided by MIT as being the growth of a condensate with an equilibrium population of about 1×10^6 atoms, at a temperature of 1200 nK [23].

In the growth experiments statistical uncertainties are estimated [25] to be 10% for relative number measurements, 15% for temperatures. Systematic uncertainties are estimated as 20% in absolute number measurements, and 8% for temperature measurements. Condensate occupations of less than 10^5 atoms could not be discerned against the background of the thermal vapor cloud [4].

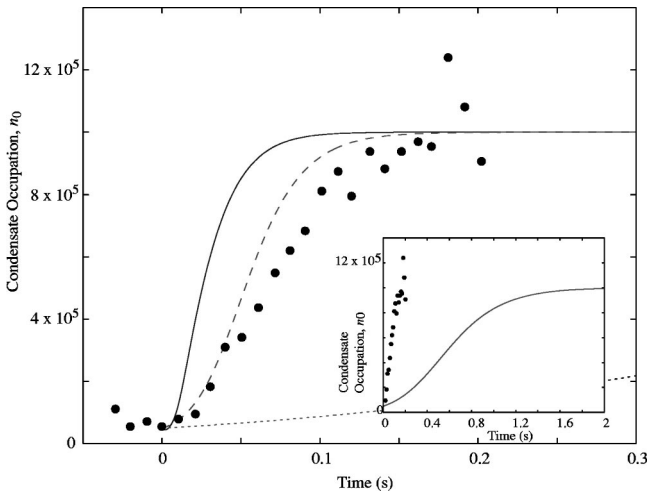

FIG. 14. Comparison of theoretical growth curves with data experimentally obtained at MIT (dots). The measured temperature for the experimental data was 1200 nK. In the main part of the figure the solid line shows the theoretical fits with standard rate constant approximations at 1200 nK, the dashed line shows the theoretical curve obtained by using $\bar{\Gamma}\Gamma(T)=\Gamma(T)/10$ and $W_m^{++}(n_0)=W^+(n_0)/2$. The dotted line shows the growth predicted by the simple growth equation of Ref. [5] [Eq. (39)], which is shown on a larger scale in the inset. The initial condensate populations for each curve were set to 5×10^4, the experimental value at $t=0$. The origin in the time axis represents the time at which the quick cooling ''cut'' in the experiment was finished.

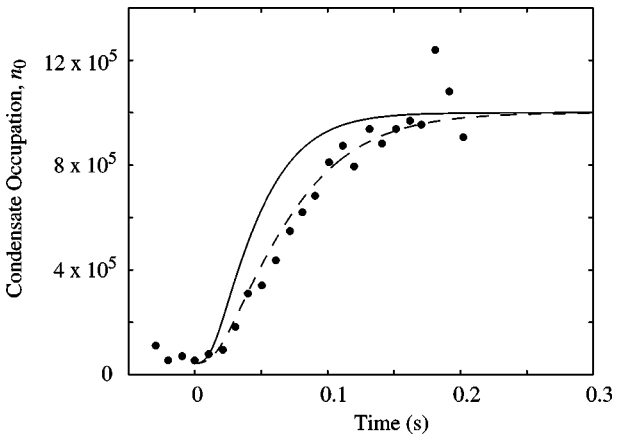

FIG. 15. Comparison of theoretical growth with MIT experimental data. The experimental data is the same as that used in Fig. 14. The theoretical curves were determined by using temperatures of 1000 nK (solid line) and 850 nK (dashed line). The rate constants were taken to be their standard values of $\bar{\Gamma}(T)=\Gamma(T)$ and $W_m^{++}(n_0)=W^+(n_0)$. Again, the initial condensate populations for each curve were set to 5×10^4.

As Fig. 14 shows, the growth predicted by our model is quite a good fit to the data, and the order of magnitude is certainly predicted well. This is a substantial improvement over the growth predicted by the simple growth equation at the same conditions which gives growth over about 1.5 s, as opposed to the experimental results of about 0.15 s. At the stated parameters the theoretical fit could still be improved. The dashed line in Fig. 14 indicates that by adjusting the scattering rate and values of W_m^{++} (as was discussed in previous sections) a better fit may be obtained.

The temperature plays a sensitive role in these comparisons, since the rate of growth is quite sensitive to temperature. Furthermore, as will be seen in Sec. IV, the fitting method may play a significant role. In Fig. 15 the theoretical curve is plotted (using the standard values of the scattering rate and W_m^{++}) for two lower temperatures. It can be seen that the fit is very good for the 850-nK results, and not quite so good, but still quite close, in the case of the 1000-nK curve.

This highlights a difficulty in comparing theoretical predictions with experimental measurements of condensate growth. The spatial density distribution of the thermal cloud (from which the temperature is measured) changes only slightly with temperature, whereas the growth rate is quite strongly dependent on the temperature. There are other problems as well, the most prominent of these being the difficulty of experimentally determining the condensate occupation. The spatial distributions of particles in the first few excited states are quite narrow functions, and they can overlap the condensate level distribution significantly. It then becomes extremely difficult to distinguish condensate level atoms from low-energy excited state atoms in experimental measurement. If the measured ''condensate occupation'' was in fact the occupation of the lowest five levels (for example), this would alter the growth curve in some important regions. The main effect would be that the growth would appear more gradual during the early times, and would not seem to have such a sharp initiation. This is a possible explanation for the S shape that was found in the MIT data. Clearly what is needed are theoretical predictions for the overall spatial density distributions during the growth, rather than merely occupation numbers for the various states. This will be addressed in Sec. IV.

The majority of the data contained in Ref. [4] were presented in the form of rate constants for fits to experimental data of the type described by Eq. (77). Figure 16 shows a comparison of our theoretical growth curves as compared to

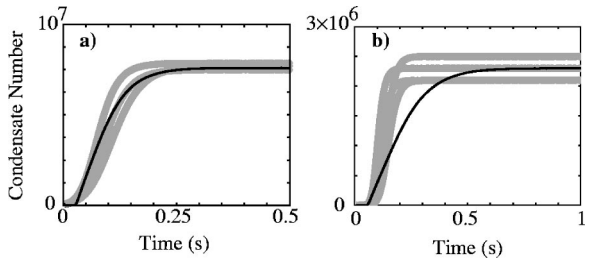

FIG. 16. Comparison of theoretical growth (thin lines) with curves fitted at MIT to experimental data in Ref. [4] (broad lines). The MIT curve fits are represented as broad lines, to indicate that they are fitted curves with unknown (but probably substantial) uncertainties. (a) Theory, $T=830$ nK, $n_{0,f}=7.6\times10^6$; experiment, $T=810$–890 nK, $n_{0,f}=(7.5$–$7.85)\times10^6$. (b) Theory, $T=590$ nK, $n_{0,f}=2.3\times10^6$; experiment, $T=580$–610 nK, $n_{0,f}=(2.1$–$2.5)\times10^6$. The initial populations were treated as free parameters to best match the initiation of the growth with the MIT curves.

solutions of Eq. (77) using a selection of the MIT fitted constants κ_1. The figure shows good overall agreement with the experimental data. The agreement is better at higher temperatures. At the lower temperatures reached in the experiment the agreement is less good.

However, the results of this paper still show an overall decrease in the the rate of growth with decreasing temperature. This is the opposite trend to that experimentally observed. This could partly be due to uncertainties in extracting numbers from the experimental data. Another possible explanation is that in order to cool to such low temperatures from just above the critical temperature in 10 ms a large proportion of the atoms must be removed. This will give rise to a system in a highly nonequilibrium state, the relaxation from which may be inadequately described by our model.

IV. SPATIAL DENSITY DISTRIBUTION OF A CONDENSATE SYSTEM

In the MIT experiments into condensate growth [4] the data were collected by phase-contrast microscopy [26,27], the measurement of change in the phase of light after it has passed through the vapor cloud. The result is a two-dimensional plot of the column density integrated along the third dimension. As discussed in Sec. III, the extraction of the population per energy level from this experimental data is complicated. Therefore, in order to more easily enable comparison with experiment, it is desirable to obtain from our theoretical results predictions of the spatial distribution of the condensate as it grows. When the system is in equilibrium this distribution is well known, but this is not the case during the condensate growth that we are interested in.

A. Semiclassical phase-space description

In order to convert the results of the model into spatial distributions, the spatial probability distributions for each energy band need to be found. The distribution for the ground state $\rho_{\rm gs}(\mathbf{r})$ is well described by the Thomas-Fermi approximation for the wave function:

$$\rho_{\rm gs}(\mathbf{r}) = |\psi_{TF}(\mathbf{r})|^2 = \frac{m}{4\pi\hbar^2 a}[\mu_C(n_0) - V_T(\mathbf{r})]\,\theta(\mu_C(n_0) - V_T(\mathbf{r})), \tag{80}$$

where $V_T(\mathbf{r})$ is the trapping potential, and $\theta(x)$ is the step function. This is a very good approximation to the shape of the condensate when n_0 is large, failing only at the very edge of the condensate where the numerical solution to the Gross-Pitaevskii equation vanishes smoothly.

A description of the spatial distributions for each of the higher-energy subbands can be found by using a semiclassical phase-space approach. The cumulative number of states below an energy E is given by

$$\mathrm{N}(E) = \frac{1}{h^3}\int d^3\mathbf{r} \int d^3\mathbf{P}\ \ \theta\left(E - \frac{P^2}{2m} - V_{\rm NC}^{\rm eff}(\mathbf{r})\right), \tag{81}$$

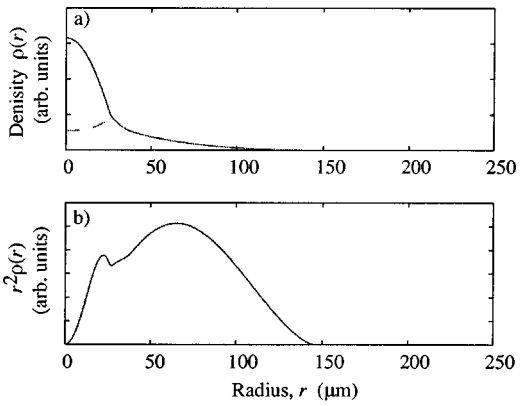

FIG. 17. Sample radial spatial density distribution for condensate having reached thermal equilibrium. (a) Solid line—total density distribution; dashed line—density distribution due to excited states only. (b) Density times radius squared. These results are for the trap parameters used in the MIT growth experiments [4,23]

where $V_{\rm NC}^{\rm eff}(\mathbf{r})$ is the effective potential experienced by an atom. This gives a density of states

$$g(E) = \frac{d\mathrm{N}(E)}{dE} = \frac{1}{h^3}\int d^3\mathbf{r} \int d^3\mathbf{P}\ \ \delta\left(E - \frac{P^2}{2m} - V_{\rm NC}^{\rm eff}(\mathbf{r})\right). \tag{82}$$

Using the local-density approximation, for an energy subband with energy e_m and width Δe_m, the average spatial distribution atoms in the band (averaged over all the wave functions of all the states in the band) may be obtained by removing the $d^3\mathbf{r}$ integral and integrating over $d^3\mathbf{P}$. This gives

$$\rho_m(\mathbf{r}) = \frac{1}{h^3}\int d^3\mathbf{P}\ \delta\left(e_m - \frac{P^2}{2m} - V_{\rm NC}^{\rm eff}(\mathbf{r})\right)\Delta e_m \tag{83}$$

$$= (4\pi 2^{1/2} m^{3/2}/h^3)\,\Delta e_m \sqrt{e_m - V_{\rm NC}^{\rm eff}(\mathbf{r})}. \tag{84}$$

1. Resulting spatial density distribution

We will use the semiclassical distributions for the excited states, and the Thomas-Fermi wave function for the condensate. The total radial probability distribution may be calculated by normalizing each level, and then summing over all the levels. The distributions are normalized so as to give the appropriate population in each level. For the bands below E_R these populations are given by the numerical results of our model. For those above E_R the population is determined by the Bose-Einstein distribution function $F(E) = [\exp((E - \mu)/kT) - 1]^{-1}$. This gives the spatial density distribution for the whole condensate system in three dimensions.

An example of the resulting spatial density distribution for a system at equilibrium is shown as Fig. 17. In the first part of this figure the total density is plotted as a function of radius, as well as the density due to the excited states only. The density due to the excited states can be seen to be significantly decreased in the region of the condensate. In Fig. 17(b) the density multiplied by the radius squared is plotted; this is proportional to the total number of atoms found at any

radius (due to the three-dimensional nature of the distribution). From this it can be seen that, even though the density in the center due to the condensate is much larger than elsewhere, the majority of the atoms are still found in the surrounding vapor cloud (as was assumed in the derivation of the model).

When the system is in equilibrium these results can be checked. At equilibrium the noncondensate spatial distribution can be obtained directly from Eq. (82). The total number of noncondensed atoms, M, is

$$M=\int_0^\infty g(\varepsilon)\frac{1}{e^{(\varepsilon-\mu)/kT}-1}d\varepsilon, \tag{85}$$

which corresponds to the local density form of $\rho(\mathbf{r})$:

$$\rho(\mathbf{r})=\frac{1}{h^3}\int d\varepsilon\int d^3\mathbf{P}\ \frac{\delta(E-P^2/2m-V_{\mathrm{NC}}^{\mathrm{eff}}(\mathbf{r}))}{e^{(\varepsilon-\mu)/kT}-1} \tag{86}$$

$$=\frac{1}{h^3}\int d^3\mathbf{P}\ \left\{\exp\left[\frac{\frac{P^2}{2m}+V_{\mathrm{NC}}^{\mathrm{eff}}(\mathbf{r})-\mu}{kT}\right]-1\right\}^{-1}. \tag{87}$$

Carrying out the integral over momentum space gives

$$\rho(\mathbf{r})=\left(\frac{mkT}{2\pi\hbar^2}\right)^{3/2}G_{3/2}\left(\frac{V_{\mathrm{NC}}^{\mathrm{eff}}(\mathbf{r})-\mu}{kT}\right), \tag{88}$$

where

$$G_\sigma(z)\equiv\sum_{n=1}^{\infty}n^{-\sigma}e^{-nz}. \tag{89}$$

A comparison of the noncondensate density obtained using Eq. (88) and that calculated by summing Eq. (84) over 1200 levels is shown in Fig. 18. It can be seen that the agreement between the two methods, for this *equilibrium* situation, is good. The agreement improves if more energy levels are included in the sum over Eq. (84), and using about 2000 levels gives very good agreement. Our semiclassical method therefore shows good agreement with the expected distribution at equilibrium, and this is the only case in which we can be certain of the theoretically correct result.

In obtaining the results in this section we have only considered effects of the mean-field repulsion due to the condensate atoms, both on the thermal vapor cloud and on the condensate itself. In order to be truly consistent the model should also include the effects of the mean-field repulsion due to the thermal cloud on the system. This is quite easily achieved mathematically, but it does increase the computational time by a very substantial amount. However, recently Naraschewski and Stamper-Kurn [28] compared the density distributions obtained both with and without considering the mean-field repulsions of the thermal cloud, for an equilibrium condensate system. They found that the overall density distributions for the two cases were practically indistinguishable except for a very small deviation at the edge of the condensate. Furthermore, Holzmann, Krauth, and Naraschewski [29] found that the semiclassical density distribution (including the mean-field repulsions by the thermal cloud) gives excellent agreement with exact quantum Monte Carlo simulations for dilute gas condensates in equilibrium. Thus we expect that the density given by our semiclassical method is a very good description of the realistic system.

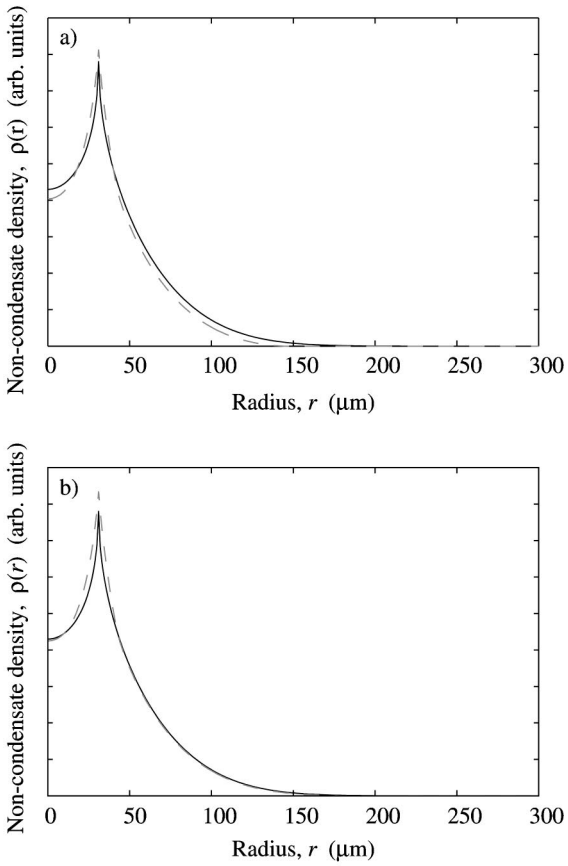

FIG. 18. Comparison of the noncondensate density distribution at equilibrium calculated (a) from the sum of 1200 individual energy level distributions (dashed), and using the $G_{3/2}(z)$ function (solid); (b) as for (a), but using the sum of 2000 energy levels.

2. Description of a realistic experimental system

The next step that must be performed, in order to compare with experimental results, is to perform a column integral along one dimension, yielding a function of two spatial dimensions only. This is relatively straightforward to achieve numerically.

Finally the asymmetry of the real traps must be taken into account. The previous arguments for the exact noninteracting wave functions assumed the use of a spherically symmetric trap, whereas the realistic traps used are strongly anisotropic in the z dimension. However, in all the previous semiclassical arguments the only effect is to change V_T from $m\omega^2r^2/2$ to $m\omega_{xy}^2(x^2+y^2)/2+m\omega_z^2z^2/2$ where now

$$\omega_{xy}=\sqrt{\lambda}\,\omega, \tag{90}$$

$$\omega_z=\omega/\lambda, \tag{91}$$

$$\omega = (\omega_x \omega_y \omega_z)^{1/3}, \tag{92}$$

$$\lambda = (\omega_x/\omega_z)^{2/3}. \tag{93}$$

Due to the harmonic nature of the trap, one can recover the original form of the potential by scaling the dimensions used. Defining

$$\overline{z} = z/\lambda, \tag{94}$$

$$\overline{x} = x\sqrt{\lambda}, \tag{95}$$

$$\overline{y} = y\sqrt{\lambda}, \tag{96}$$

the potential now returns to the form $V_T(\overline{\mathbf{r}}) = m\omega^2\overline{r}^2/2$, where the scaled radius is given by $\overline{r} = \sqrt{\overline{x}^2 + \overline{y}^2 + \overline{z}^2}$. Equation (84) can now still be used, and the column density integration performed as for an isotropic potential, and the resulting function of $\overline{x}$ and $\overline{z}$ needs only to be rescaled to recover the answer in terms of x and z. This scaling also affects the numerical column integration, with the effect that the result needs to be scaled overall by a factor of $\lambda^{-1/2}$ [assuming the integration is in one of the two shorter dimensions and that the result is in the asymmetric (longer) dimension, as is the case for the ''cigar'' geometry traps of MIT].

B. MIT fitting method

In the MIT experiments, the data for the numbers of condensate atoms and temperatures are obtained from fitting to the density profile obtained. The raw data obtained are in the form of two-dimensional images and, although these can be fitted, in order to save time and computational resources the fit was mostly performed only to a one-dimensional slice through the center of the condensate [23]. This density profile is fitted from a function formed by the combination of a condensate density profile and noncondensate profile. The MIT fitting procedure is a phenomenological procedure which neglects interactions between the condensate and the vapor. It is based on two observations:

(i) The behavior of the thermal cloud in the wings of the profile is almost independent of the chemical potential—its behavior in the wings can thus be used to determine the temperature of the vapor.

(ii) The center of the profile is dominated by the condensate, and this—after subtracting the contribution of the vapor—can be fitted to the parabolic Thomas-Fermi profile, to determine the condensate chemical potential and thus the number in the condensate.

The explicit procedure actually used was not clearly described in Ref. [4], but was described in full in Ref. [7]. In this particular experiment a linear combination of a Thomas-Fermi function and a $\mu = 0$ Bose-Einstein distribution was fitted to the observed profile using a procedure which, using our notation, takes the following form. For that part of the density due to the vapor (or noncondensate), one sets the chemical potential to zero and integrating along one dimension gives a contribution to the column density (for a slice where $x = 0$) of the form

$$\rho_{\mathrm{int},V}(z, x=0) = \int_{-\infty}^{\infty} \rho_V(z, y, x=0)\, dy \tag{97}$$

$$= \frac{m(kT)^2}{2\pi\hbar^3\omega_y} G_2\left(\frac{m\omega_z^2}{2kT} z^2\right). \tag{98}$$

The column density function due to the condensate, $\rho_{\mathrm{int},C}$, is obtained by integrating the Thomas-Fermi wave function given by Eq. (80) over one dimension,

$$\rho_{\mathrm{int},C}(z, x=0) = \int_{-y_1(z)}^{y_1(z)} \left[\frac{\mu_C(n_0)}{u} - \frac{m}{2u}(\omega_z^2 z^2 + \omega_y^2 y^2)\right] dy, \tag{99}$$

where

$$y_1(z) = \sqrt{\frac{2\mu_C(n_0)}{m\omega_y^2} - \frac{\omega_z^2}{\omega_y^2} z^2}, \tag{100}$$

and where $u = 4\pi\hbar^2 a/m$, giving

$$\rho_{\mathrm{int},C}(z, x=0) = \frac{2m\omega_y^2}{3u}\left(\frac{2\mu_C(n_0)}{m\omega_y^2} - \frac{\omega_z^2}{\omega_y^2} z^2\right)^{3/2}. \tag{101}$$

In the measurement procedure used, the phase-shift data were not calibrated independently. The phase-shift data, which we shall call $\mathrm{Ph}(z)$, were fitted to a *linear combination* of the form

$$\mathrm{Ph}(z) = S_V \rho_{\mathrm{int},V} + S_C \rho_{\mathrm{int},C}. \tag{102}$$

There are thus *two independent scale factors* S_V and S_C which relate the observed profile to the fit functions. The number of condensate atoms was obtained from the spatial width z_0 of the Thomas-Fermi function $\rho_{\mathrm{int},C}$. These are related by

$$\rho_{\mathrm{int},C}(z_0, x=0) = 0 \tag{103}$$

when

$$z_0^2 = \frac{2\mu_C(n_0)}{m\omega_z^2} = \left(\frac{15u(m/2)^{3/2}\overline{\omega}^3}{8\pi}\right)^{2/5} \frac{2n_0^{2/5}}{m\omega_z^2}; \tag{104}$$

thus $n_0 \propto z_0^5$.

This fitting method was found to give very good fits to the phase-shift data obtained. However, it has no fundamental basis, and in particular the identification of the fitted Thomas-Fermi shape with the condensate itself is not easy to justify when independent scale factors as in Eq. (102) are used.

C. Comparison of fitting methods

In Fig. 19 we show a least-squares fit of a linear combination of a zero chemical potential and a Thomas-Fermi con-

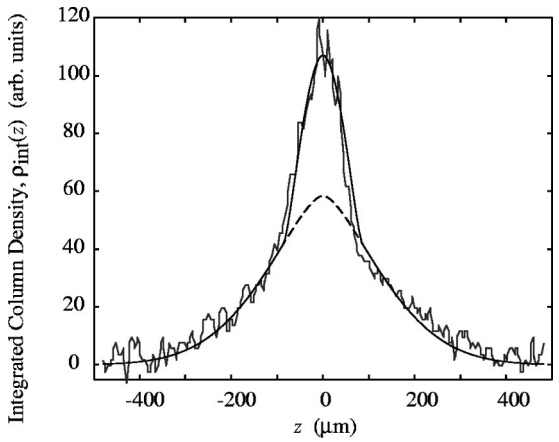

FIG. 19. Equilibrium data obtained from MIT [4] fitted using the MIT procedure as described in the text (solid smooth curve), and showing the component due to the noncondensate (dashed line). Parameters used were $T=800$ nK, 9 000 000 condensate atoms. The density scale factors were 1.08×10^{-14} for the condensate, and 2.85×10^{-14} for the vapor.

densate profile—that is, of the form Eq. (102)—for an equilibrium distribution. The data used was obtained from Fig. 2 of Ref. [4], for which the MIT group obtained values of $T=800$ nK with 9 000 000 condensate atoms present in equilibrium after 160 ms [23]. Also shown is the contribution to the distribution due to the noncondensate atoms only. Note that the z axis has been scaled by a factor of 3.2 over that in Ref. [4], correcting a typographical error [23].

In this fit, as for all the following cases, the density scale factors (necessary to convert from the arbitrary unit scale resulting from the experimental measurements) were determined by the least-squares fitting procedure. Since we use the T and n_0 determined by the MIT group using their procedure, these two scale factors are the only free parameters

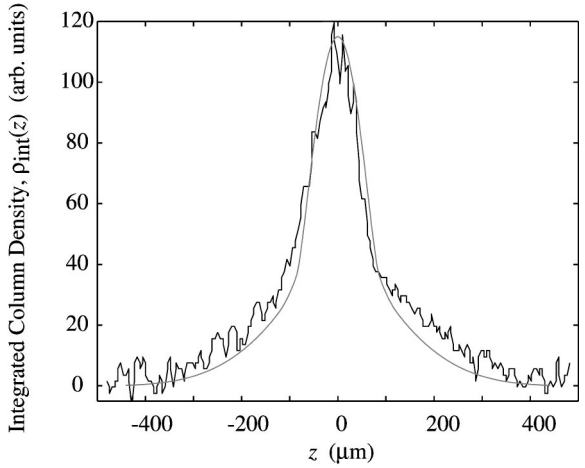

FIG. 20. Equilibrium data as for the previous figure, fitted by using the semiclassical method proposed in this paper. Temperature and number of condensate atoms were taken to be the same as was used previously ($T=800$ nK and $n_0=9\times10^6$); however, the density scale factor was changed to 1.71×10^{-14}.

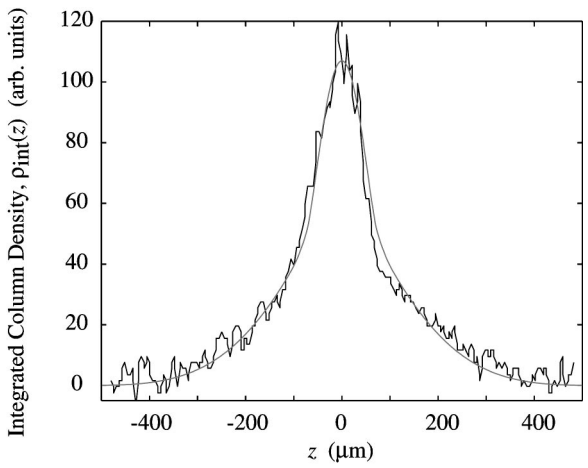

FIG. 21. The best fit to the same data used in the previous two figures. The parameters used were $T=900$ K, $n_0=4\times10^6$ and the density scale factor was 1.96×10^{-14}.

in this fit. The fit is very good, but it should be noted that the scale factors differ by a factor of more than 2.

The same data can be fitted using the distributions from Eq. (84). Figure 20 shows the same equilibrium data, fitted by using the same parameters but by using the semiclassical distribution—as before, we use the T and n_0 determined by the MIT group using their procedure, so that the only free parameter is a *single* scale factor. This spatial distribution does not fit the experimental data so well. However, if we allow T and n_0 to be determined by *our* fitting procedure, we obtain a very good fit. The best fit was found with parameters of $T=900$ nK with 4 000 000 condensate atoms and a density scale factor of 1.96×10^{-14}, and is shown in Fig. 21. The temperature determined by our method at 900 K is not

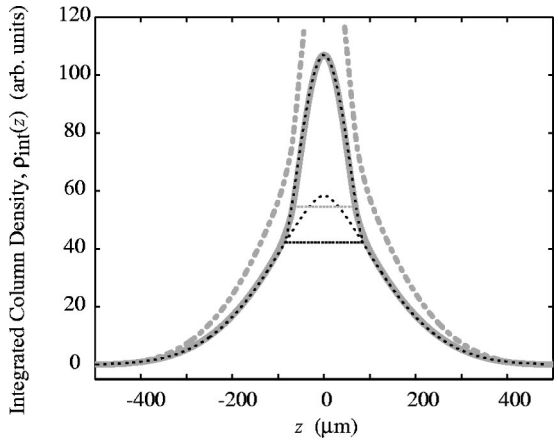

FIG. 22. Comparison of the two fit functions: (a) Dashed line: the MIT zero chemical potential vapor fit as in Fig. 19. (b) Gray solid line: our best fit as in Fig. 21. The horizontal dotted lines represent the widths of the Thomas-Fermi condensate functions for the two cases. (c) Gray dot-dashed line: this represents the MIT fit, but plotted using the same scale factor for the thermal cloud (and an appropriately adjusted factor for the condensate) as for our fit, in order to demonstrate that although the shapes of the two fits are the same, they do represent different physics.

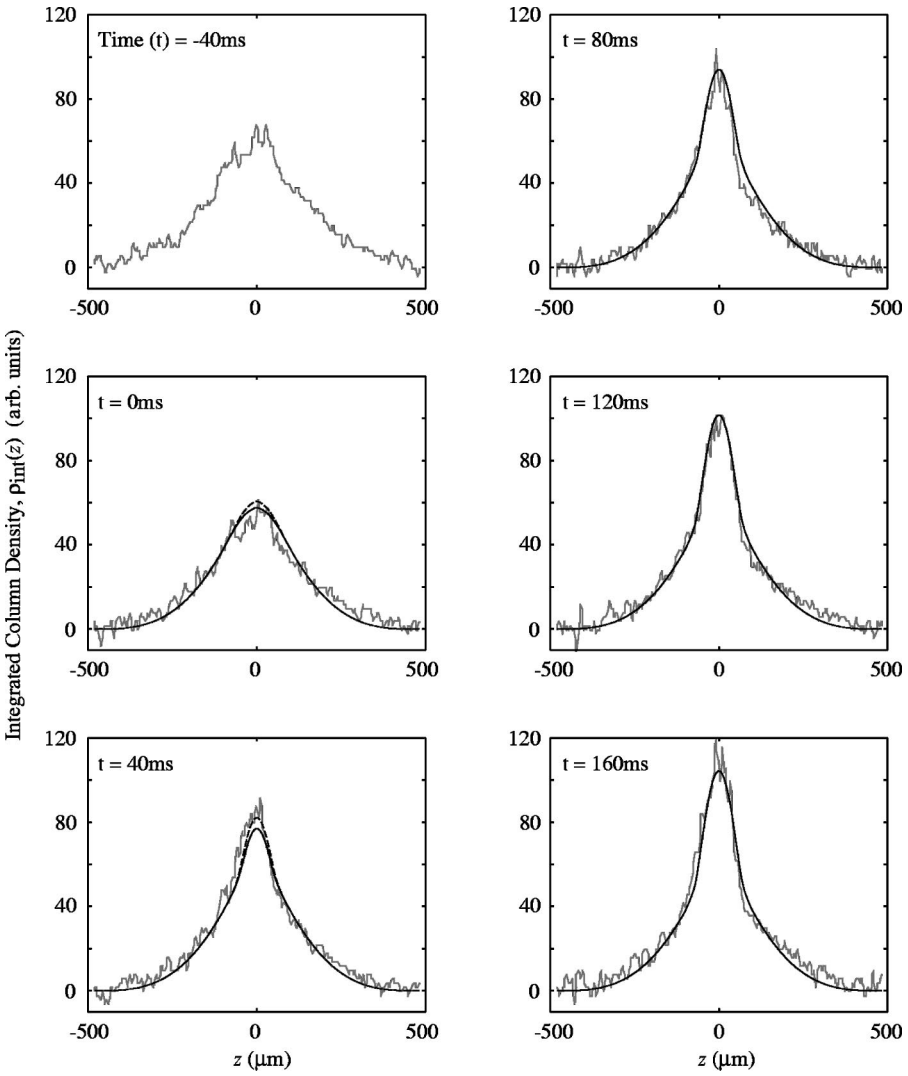

FIG. 23. Comparison between experimental data from Ref. [4] and theoretical spatial density distributions, calculated using the semiclassical density distributions and the growth model described in this paper. The scale factor is 1.96×10^{-14}. The first frame shows the distribution before the cooling ''cut'' below the critical temperature was performed. The parameters used were $T=900$ nK and $n_{0,f}=4\times10^{6}$. The (lower) solid curves show the theoretical curves using initial condition (c) described in Sec. III A 6. In the second and third frames the (upper) dashed curves depict the results obtained using initial condition (d) which become essentially indistinguishable from the condition (c) curves for the final three profiles.

very different from the 800 K determined by the MIT procedure, but the condensate number by our method is, at 4×10^{6}, less than half of the MIT value of 9×10^{6}.

In order to compare the MIT fit and our best fit, we have plotted the two fit functions on the same graph in Fig. 22. As can be seen, the two are almost indistinguishable. However, the fact that the condensate numbers differ by a factor of 2 shows that the assumption that the width of the ''condensate'' peak in the MIT fit determines the condensate number is not justified here.

The MIT fit manages to produce almost exactly the correct profile as follows. Our profile has rather distinct ''shoulders'' adjacent to the condensate peak, which merge rather smoothly into the condensate peak. This behavior is mimicked in the MIT fit by lowering the temperature of the vapor by about 10%, which tends to make the vapor cloud rise more rapidly as one approaches the center of the trap, and by broadening slightly and flattening considerably the condensate peak. At the same time, the ''shoulders'' in our fit are continued further into the system, until the true narrower and smaller condensate peak occurs. The actual peak widths differ by about 18%, which then produces the change in condensate number of 220% because of the fifth power relationship between the peak width and the condensate number.

D. Analysis of spatial distributions of the growing condensate

With the aid of the spatial distributions calculated using Eq. (84), comparisons with the MIT growth data are possible. In Fig. 2 of Ref. [4] the density profiles of the system are given for a single condensate growth run, and these are reproduced here in Fig. 23. The profiles are one-dimensional slices through the center of the system, in the z (long) axis. In addition to this graphical information, we also have the knowledge that after the final profile, at $t=160$ ms, no further growth was observed to occur [23]. (The first profile, at $t=-40$ ms, is taken before the rf cut, is thus not part of the growth sequence, and is not included in our fits).

The final profile can therefore be taken to correspond to thermodynamic equilibrium, and the fits to the equilibrium profile were compared in Sec. IV C. From this data, MIT extracted values of $T=800$ nK and $n_{0,f}=9\times10^{6}$. If these values are used to compute the corresponding growth curve, it is found that the predicted growth does not cease at $t=160$ ms, but instead continues until at least $t=250$ ms.

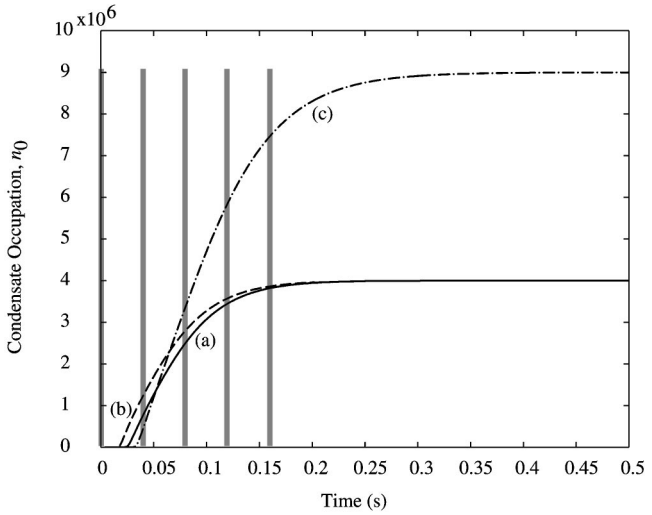

FIG. 24. Condensate growth curves corresponding to the fits to the growth data of Fig. 23. (a) (Solid line) and (b) (dashed line): fits with $T=900$ nK and $n_{0,f}=4\times10^6$ with initial conditions (c) and (d) of Fig. 11. (c) (Dot-dashed line): fit using the MIT value $T=800$ nK and $n_{0,f}=8\times10^6$. Gray vertical lines indicate the times at which the profiles were taken.

Nevertheless, using a single scale factor, a fit can be found to the five growth profiles by using the procedure described in Sec. IV A, with the condensate number of the final profile, at $t=160$ ms, given by $n_0=7.5\times10^6$. However, the predicted profiles for subsequent times up to about 250 ms show significant further development (corresponding to the fact that the condensate number n_0 must continue to grow to reach its ultimate value of 9×10^6), in contradiction to the observation that no further growth occurs.

If instead we use parameters corresponding to our best fit to the equilibrium data, namely $n_{0,f}=4\times10^6$ and $T=900$ nK, the predicted growth is faster, and growth is in fact complete at $t=160$ ms, as can be seen in condensate growth curve given in Fig. 24. Using a single scale factor for all five profiles a very good fit is found for the last five profiles by using the procedure described in Sec. IV A—the theoretical spatial distribution curves are compared to the experimental data in Fig. 23. Taking the variance of the data points to be about 20, we find $\chi^2=1300$ for this fit, which is to be compared to an expected $\chi^2=1272\pm50$, whereas the fit assuming that the growth curve and profiles are characterized by $n_{0,f}=9\times10^6$ and $T=800$ nK has $\chi^2=2575$—that is, the χ^2 is 24 standard deviations from the expected value. This corresponds to a speedup by a factor of about 1.5, which is of the order of magnitude of some of those found in our fits in the previous section, and has two basic causes:

(i) The higher temperature increases the intrinsic growth rate which is roughly proportional to T^2.

(ii) Although the lower final number, $n_{0,f}$—reduced by a factor of about 2—reduces the gain slightly, this is far outweighed by the need for the growth curve to rise less than half the height.

The frame at 40ms shows the least good agreement; however, the agreement can be improved by the choice of different initial conditions, as is shown in Fig. 23. Using initial condition (d), described in Sec. III A 6, the agreement with experiment again becomes very impressive. It is interesting to note that the spatial density distribution in this frame depends significantly on the initial conditions, which were found to have only a very small effect on the growth curve in Sec. III A 6. This is because the 40-ms frame is taken at a time very close to the initiation of the fast growth of the condensate population, and the spatial distribution at this time is quite strongly dependent on exactly when the growth does start, since any difference in the initiation time creates a relatively large change in the occupation numbers which are still quite low at this time.

E. Conclusions

The conclusions of this section depend on the use of the single set of growth profiles which has been published, but are consistent and convincing.

(i) The phenomenological MIT fitting procedure appears to overestimate the condensate number by a factor of 2, and to give a temperature about 10% too small.

(ii) Quite independently, the time of growth predicted using the parameters extracted by MIT fitting procedure is too slow by a factor of about 1.5.

(iii) However, fitting the same data using the theoretically correct profiles gives values of temperature and final condensate number which lead to a growth curve in agreement with the experimental data for the growing condensate profiles.

It is possible that this is the source of the apparent speedup found in many of the growth curves, for which spatial profiles are not available. However, it is emphasized by the experimenters [25] that the phase contrast data used in these fits probably requires additional correction to take account of finite optical resolution and scattering effects, and that these corrections—although probably quite minor—could well be different for the condensate and vapor profiles, which have very different shapes, sizes, and densities.

It is clear that the lack of any independent calibration of the phase contrast determination of column density is the major source of uncertainty in the interpretation of the data. The wide range of scale factors found would be eliminated by such a calibration.

V. COMPARISON WITH OTHER THEORETICAL TREATMENTS

Most of the other theoretical treatments have attempted to describe the formation of a condensate in a homogeneous, untrapped situation. No real quantitative predictions have yet emerged from any of the work that has been performed on trapped dilute atomic gas Bose-Einstein condensation, and so comparisons unfortunately will have to be qualitative at best.

A. Quantum Boltzmann equation approach

One of the techniques used to describe condensate growth has been the quantum Boltzmann equation, which has been used by Snoke and Wolfe [30], Semikoz and Tkachev [31], and Holland, Williams, and Cooper [21], as well as forming the basis of the theory of the kinetic stages in the work of

Kagan, Svistunov and Shlyapnikov [32,33]. Although the theory described in this paper was developed from the quantum Kinetic theory [10–12], it turns out that essentially the same equations may be obtained by modifying the quantum Boltzmann equation approach as follows:

(i) The quantum Boltzmann equation in an ergodic form is used, a form similar to that used in Ref. [21],

$$\frac{\partial f(e_n)}{\partial t}=\frac{8ma^2\omega^2}{\pi\hbar}\sum_{e_m,e_p,e_q}\delta(\Delta E)g(e_{\min}) \times[f(e_p)f(e_q)(1+f(e_m))(1+f(e_n)) -f(e_m)f(e_n)(1+f(e_p))(1+f(e_q))], \quad (105)$$

where $n_k=g_kf(e_k)$ is the number of particles with energy e_k, $e_{\min}=\min(e_m,e_n,e_p,e_q)$ and $\Delta E=e_m+e_n-e_p-e_q$.

(ii) The energy levels in the condensate band are modified as discussed in Sec. III A 7, in order to account for the mean-field interactions due to the presence of the condensate.

(iii) The levels in the noncondensate band are summed over and assumed to be time independent. This allows much larger, and realistic sized, systems to be modeled as opposed to the 100–1000 atom systems typically simulated in previous attempts.

(iv) Collisions between two particles which were both initially in the condensate band were neglected, this is a valid approximation if the vast majority of particles are found in the noncondensate band.

Using these modifications, and the rates for the scattering and growth processes found from quantum kinetic theory (see Sec. II F), the quantum Boltzmann equation will give rise to the set of differential equations (72) whose solutions provided the results in this paper.

Of the above references, only the work of Holland, Williams, and Cooper conducted any simulations for the growth of a trapped condensate. They found that their simulations of condensate occupation number evolution behaved as $n_0=n_{0,f}(1-e^{-t/\tau})$, where τ was a fitted parameter. A function of this form can be made to fit the results obtained by our model reasonably well, provided that an initiation time is allowed for, as was anticipated might be necessary in Ref. [21]. The same functional form was obtained using the quantum Boltzmann master equation approach in Ref. [11] by Jaksch *et al.*

It should be noted that, although the quantum kinetic description for the growth of the *mean* occupation numbers also turns out to be described by a modified quantum Boltzmann equation approach, the full quantum kinetic theory treats aspects of condensate dynamics which are not accessible via the quantum Boltzmann equation. Such aspects include the treatment of fluctuations, phase and phase decoherence, and the inclusion of Bogoliubov-like quasiparticle states.

B. Comparison with work of Kagan *et al.*

Major theoretical work into the growth of condensate in recent years has been performed by Kagan, Svistunov, and Shlyapnikov. They divided the growth into three stages, the first of which was a kinetic stage described by Svistunov in Ref. [32]. Svistunov predicted the formation of a particle-flux wave in energy space during the initial stages, which transports particles toward lower-energy states. The arrival of this wave at the lowest-energy state at the *critical time* would give rise to an energy distribution function of the form $f(E)\propto E^{-7/6}$. After the critical time this behavior would be lost due to a particle-flux wave propagating to higher energies. The simulations of Semikoz and Tkachev [31] showed this behavior to some extent, although they found that the behavior at the critical time was $f(E)\propto E^{-1.24}$.

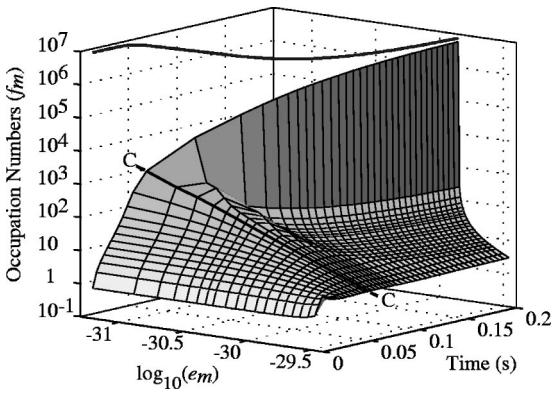

FIG. 25. The growth of a condensate of 9 000 000 atoms, as predicted by the model in this paper. Plotted is $f(e_m)$, the population per individual level with energy e_m, and the energies of the levels as functions of time. The values of $f(e_m)$ and e_m are plotted on log scales. The lines almost parallel to the time axis are not lines of constant energy, but rather lines of constant level number, whose energies change with time. Not all levels are shown in order to make the behavior legible. The solid black curve represents the energy of the condensate level $\log_{10}[\mu_N(n_0)]$ as a function of time. The bold line labeled *C-C* represents the critical time, at which the energy distribution has the form $f(E)\propto E^{-1.61}$. The temperature of the system was 800 nK.

The work by Svistunov in Ref. [32] related to the case of homogeneous systems; however, he recently reworked his methodology to consider a gas confined by a harmonic trapping potential. In this case he found [34] that the dependence at the critical time now tended toward $f(E)\propto E^{-5/3}$.

In Fig. 25 the results our model of condensate growth are shown in a somewhat different form. The occupation numbers for both the condensate level and excited states are plotted as a function of their energy and the time (note the logarithmic scales). From this graph several points can be noted. First, the front corner shows quite how rapidly the initial conditions, however arbitrary, are smoothed out by scattering processes, and the discontinuous initial conditions rapidly approach a realistic distribution. The growth of the condensate is rather small up to the point labeled as the critical time, after which the condensate grows enormously. The populations of the excited states approach equilibrium very rapidly after the critical time, much more rapidly than the condensate level does.

As the critical time is approached, the distribution approaches a straight line as shown in Fig. 25. At the critical time, when this distribution is linear with the logarithm of

the energy, the energy dependence was found to be of the form $f(E) \propto E^{-1.61}$, which is in good agreement with the prediction of Svistunov of $E^{-5/3}$.

As far as estimates of time scales are concerned, Kagan, Svistunov, and Shlyapnikov predicted that the evolution of the system up until initiation would occur on the time scale of the classical collision time τ_0, that the initiation of the condensate growth would occur on a much faster time scale, and that the final growth would occur on the time scale necessary for the annihilation of vortices in homogeneous gases, and the decay of fluctuations in the phase of the condensate.

In the treatment of Kagan, Svistunov, and Shlyapnikov the time scale for the first kinetic stage was postulated for a homogeneous gas; however, a comparison can still be made. A first estimate of $\tau_0 = (\sigma \bar{n} v_T)^{-1}$ can be obtained by using the classical value for v_T, the mean thermal velocity in a gas, of $v_T = \sqrt{2kT/m}$, and the cross section defined by $\sigma = 8\pi a^2$. The value for $\bar{n}$, the mean density, will be taken as the density of the noncondensate particles in the center of the trap given by

$$\bar{n} = \left[\frac{mkT}{2\pi\hbar^2}\right]^{3/2} G_{3/2}\left(\frac{V_T(0)}{kT}\right) \tag{106}$$

[see Eq. 88], where $G_\alpha(z) = \Sigma_{q=1}^{\infty} e^{-qz}/q^\alpha$. Taking $V_T(0) = 0$, and using a temperature of 900 nK, the collision time is $\tau_0 = 27$ ms. This temperature corresponds to that of the growth in Fig. 8, which shows that the time until initiation is of the order of $2\tau_0$. Thus our treatment does agree with the picture of Kagan *et al.* in that this stage occurs over the order of a few τ_0.

A note about the collision times is needed here. In examining the validity of the ergodic approximation, Jaksch *et al.* found that it was valid only for quantities averaged over about ten collision times [11]. The above time scale τ_0 is *not* the time scale over which collisions occur in the condensate system in reality. It is rather the classical collision time for a classical gas in equilibrium below the critical temperature but with *no* condensate present, and is obviously artificial. Once the condensate begins to form, the density increases significantly, and the actual mean collision time was found in Ref. [11] to be more than two orders of magnitude smaller than τ_0. Thus the ergodic assumption should still be valid for our treatment, even given the large value of τ_0.

The time scales found by Kagan *et al.* for the second and third stages of evolution have only been determined for the case of a homogeneous gas, and so accurate comparisons with our model for these stages are not able to be performed. Our model does agree that the initiation stage occurs on a much faster time scale than the first kinetic stage. The presence of vortices has not been considered in our treatment, nor has any consideration been given to the phase fluctuations, and so comparisons cannot be made with the third stage of evolution in the description of Kagan *et al.*

VI. CONCLUSIONS

In this paper a model of the growth of a condensate, derived from quantum kinetic theory [10–12], is presented. The main improvements over the simpler description in Ref. [5] are the more accurate calculation of the growth rate factor $W^+(n_0)$, the consideration of the time dependence of the lower-energy levels, and the inclusion of the scattering of particles between these levels. The modified W^+ factors have the greatest effect, generally increasing the rate of growth by a factor of about 3, dependent on the exact parameters. The inclusion of the other levels and their scattering also leads to an increase in the rate of growth, mainly by reducing the amount of time taken for the initiation of the growth; that is, the time before the stimulated growth processes, due to the Bose statistics of the system, become dominant.

The model describes the evolution of time-dependent energy levels in the lowest states, coupled with a time independent thermal bath of atoms occupying the higher-energy levels. The results give growth curves whose shapes are approximately those given by

$$n_0 = \begin{cases} 0 & \text{for } t < t_i \\ n_{0,f}(1 - e^{-(t-t_i)/\tau}) & \text{for } t > t_i, \end{cases} \tag{107}$$

where t_i is some initiation time. This form agrees with the general form of the results of Holland *et al.* [21] and Jaksch *et al.* [11] once an initiation time is allowed. The results also seem to be in qualitative agreement with features of the description proposed by Kagan, Svistunov and Shylapnikov.

The results are not very sensitive to the exact nature in which the mean-field effects on the lower levels were accounted for, so long as the energies of the very lowest levels were altered in a consistent fashion. The initial conditions used did not have a large effect on the growth curves, however they can be important when the spatial density profiles of the system are calculated for comparison with experiment.

The evolution of the model depends upon approximations made for the rate factors $\Gamma(T)$ and $W_m^{++}(n_0)$. The results obtained show that the growth is not very different as long as the actual value of $\Gamma(T)$ falls within about a factor of 10 of the approximation, and as long as the actual values of $W_m^{++}(n_0)$ lies within a factor of 2 of $W^+(n_0)$.

Overall the rates of growth predicted now agree rather well with the growth rates measured from experimental data [4]. However, at lower temperatures the trend in growth rates shows some divergence, with the experimental rates becoming quicker while the predicted rates become slower. This may be a result of the substantial cooling necessary to achieve these temperatures, giving rise to a highly nonequilibrium system which is inadequately described by our model.

However, it could also be related to the use of the MIT phenomenogical fitting procedure by which condensate numbers and temperatures have been extracted from the condensate profiles in the experiment, since our method of extracting these data, as given in Sec. IV, has a reasonably sound theoretical basis, and gives considerably different values of the condensate number, and somewhat different values of temperature, from the method used in the experiment. In the one set of experimental profile data which we have been able

to check, only the values given by our method give a growth curve which fits the profile data. The values given by the MIT method give a theoretical growth rate which is too slow by a factor of about 1.5—in other words, an apparent speedup of the experimental condensate growth by a factor of 1.5, caused by the underestimate of condensate number and vapor temperature which result from the phenomenological fitting procedure used.

Further work which could be undertaken within the framework of this model includes the following.

(i) An accurate determination of the rate factors $\Gamma(T)$ and $W_m^{++}(n_0)$ analytically, or at least finding constraints on their values by comparison with more experimental data.

(ii) An inclusion of some Bogoliubov phononlike quasiparticle nature in the description of the lower-energy levels, since all excited levels in this paper were treated as Hartree-Fock particlelike quasiparticles, which will be valid for most of the higher levels but not for the lower-energy excitations.

(iii) A consideration of the fluctuations in occupation numbers. These may be significant in determining the initiation time, which is when the occupation of the condensate level becomes large enough for the stimulated growth processes to take over.

(iv) As the model stands, the noncondensate band ''bath'' of atoms is treated as being time independent. A major extension of the model would be to include the dynamics of the noncondensate band in the evolution. Extension to include a time-dependent bath will be treated elsewhere [35].

ACKNOWLEDGMENTS

We would especially like to thank Wolfgang Ketterle and Hans-Joachim Miesner for discussions regarding the interpretation of their data, as well as Yuri Kagan and Boris Svistunov for discussions concerning their work on the kinetic theory of condensate initiation. The research was supported by the Royal Society of New Zealand under Marsden Fund Contract Nos. PVT-603 and PVT-902.

[1] M. Anderson, J. R. Ensher, M. R. Matthews, C. E. Wieman, and E. A. Cornell, Science **269**, 198 (1995).
[2] K. B. Davis, M-O. Mewes, M. R. Andrews, N. J. van Druten, D. S. Durfee, D. M. Kurn, and W. Ketterle, Phys. Rev. Lett. **75**, 3969 (1995).
[3] C. C. Bradley, C. A. Sackett, J. J. Tollet, and R. Hulet, Phys. Rev. Lett. **75**, 1687 (1995).
[4] H.-J. Miesner, D. M. Stamper-Kurn, M. R. Andrews, D. S. Durfee, S. Inouye, and W. Ketterle, Science **279**, 1005 (1998).
[5] C. W. Gardiner, P. Zoller, R. J. Ballagh, and M. J. Davis, Phys. Rev. Lett. **79**, 1793 (1997).
[6] C. W. Gardiner, M. D. Lee, R. J. Ballagh, M. J. Davis, and P. Zoller, Phys. Rev. Lett. **81**, 5266 (1998).
[7] W. Ketterle, D. S. Durfee, and D. M. Stamper-Kurn, in *Proceedings of the International School of Physics ''Enrico Fermi'' Course CXL*, edited by M. Inguscio, S. Stringari, and C. Wieman (IOS Press, Amsterdam, 1999).
[8] D. G. Fried *et al.*, Phys. Rev. Lett. **81**, 3811 (1998).
[9] In this paper will use the notations QKI for Ref. [10], QKII for Ref. [11], QKIII for Ref. [12], QKIV for Ref. [13], and QKV for Ref. [14].
[10] C. W. Gardiner and P. Zoller, Phys. Rev. A **55**, 2902 (1997).
[11] D. Jaksch, C. W. Gardiner, and P. Zoller, Phys. Rev. A **56**, 575 (1997).
[12] C. W. Gardiner and P. Zoller, Phys. Rev. A **58**, 536 (1998).
[13] D. Jaksch, C. W. Gardiner, K. M. Gheri, and P. Zoller, Phys. Rev. A **58**, 1450 (1997).
[14] C. W. Gardiner and P. Zoller, Phys. Rev. A **61**, 033601 (2000).
[15] F. Dalfovo, S. Giorgini, L. P. Pitaevskii, and S. Stringari, Rev. Mod. Phys. **71**, 463 (1999).
[16] F. Dalfovo, S. Giorgini, M. Guilleumas, L. Pitaevskii, and S. Stringari, Phys. Rev. A **56**, 3840 (1997).
[17] C. W. Gardiner, Phys. Rev. A **56**, 1414 (1997).
[18] M. J. Davis (personal communication).
[19] A. Erdelyi *et al.*, *Higher Transcendental Functions* (McGraw-Hill, New York, 1953), Vol. 1.
[20] C. W. Gardiner and P. Zoller, *Quantum Noise*, 2nd ed. (Springer-Verlag, Berlin, 1999).
[21] M. Holland, J. Williams, and J. Cooper, Phys. Rev. A **55**, 3670 (1997).
[22] E. Tiesinga, C. J. Williams, P. S. Julienne, K. M. Jones, P. D. Lett, and W. D. Phillips, J. Res. Natl. Inst. Stand. Technol. **101**, 505 (1996).
[23] H.-J. Miesner (personal communication).
[24] Yu. Kagan and B. V. Svistunov, Phys. Rev. Lett. **79**, 3331 (1997).
[25] W. Ketterle (personal communication).
[26] M. R. Andrews, M.-O. Mewes, N. J. van Druten, D. S. Durfee, D. M. Kurn, and W. Ketterle, Science **273**, 84 (1996).
[27] M. R. Andrews, D. M. Kurn, H.-J. Miesner, D. S. Durfee, C. G. Townsend, S. Inouye, and W. Ketterle, Phys. Rev. Lett. **79**, 553 (1997).
[28] M. Naraschewski and D. M. Stamper-Kurn, Phys. Rev. A **58**, 2423 (1998).
[29] M. Holzmann, W. Krauth, and M. Naraschewski, Phys. Rev. A **59**, 2956 (1999).
[30] D. W. Snoke and J. P. Wolfe, Phys. Rev. B **39**, 4030 (1989).
[31] D. V. Semikoz and I. I. Tkachev, Phys. Rev. Lett. **74**, 3093 (1995).
[32] B. V. Svistunov, J. Mosc. Phys. Soc. **1**, 373 (1991).
[33] Yu. Kagan, B. V. Svistunov, and G. V. Shlyapnikov, Zh. Éksp. Teor. Fiz. **101**, 528 (1992) [Sov. Phys. JETP **75**, 387 (1992)].
[34] B. V. Svistunov (personal communication).
[35] M. J. Davis, C. W. Gardiner, and R. J. Ballagh, e-print cond-mat/9912439.